EMU Notes in Mineralogy, Vol. 20 (2019), Chapter 6, 233–281

The struggle between thermodynamics and kinetics: Phase evolution of ancient and historical ceramics

ROBERT B. HEIMANN[1] and MARINO MAGGETTI[2]

[1]*Am Stadtpark 2A, D-02826 Görlitz, Germany*
robert.heimann@ocean-gate.de
[2]*University of Fribourg, Dept. of Geosciences, Earth Sciences, Chemin du Musée 6, CH-1700 Fribourg, Switzerland*
marino.maggetti@unifr.ch

This contribution is dedicated to the memory of Professor Ursula Martius Franklin, a true pioneer of archaeometric research, who passed away at her home in Toronto on July 22, 2016, at the age of 94.

Making ceramics by firing of clay is essentially a reversal of the natural weathering process of rocks. Millennia ago, potters invented simple pyrotechnologies to recombine the chemical compounds once separated by weathering in order to obtain what is more or less a rock-like product shaped and decorated according to need and preference. Whereas Nature reconsolidates clays by long-term diagenetic or metamorphic transformation processes, potters exploit a 'short-cut' of these processes that affects the state of equilibrium of the system being transformed thermally. This 'short-cut' is thought to be akin to the development of mineral-reaction textures resulting from disequilibria established during rapidly heated pyrometamorphic events (Grapes, 2006) involving contact aureoles or reactions with xenoliths. In contrast to most naturally consolidated clays, the solidified rock-like ceramic material inherits non-equilibrium and statistical states best described as 'frozen-in'. The more or less high temperatures applied to clays during ceramic firing result in a distinct state of sintering that is dependent on the firing temperature, the duration of firing, the firing atmosphere, and the composition and grain-size distribution of the clay. Hence, the salient properties of the ceramics have to be assessed in a temperature-time-composition space. Owing to the variability of clay composition, the mineralogical processes during thermal transformation of clay minerals can be very complex, not least because most reactions occur far removed from thermodynamic equilibrium and hence are kinetically controlled; that is, they are time- and temperature-dependent. Indeed, kinetics imposes constraints on thermodynamics by retarding reaction rates because of low temperatures, large temperature gradients present in primitive pottery kilns, short reaction times, inhomogeneously distributed reaction partners, and varying redox conditions triggered, for example, by ingress of air during reducing firing cycles. In the context of ceramic technological development over time, the role and development of pottery technology within complex societies is discussed. The close relationship between pottery development and changes in life/societal organization appears to be a major driver in this endeavour.

In this chapter, the phase evolution of some typical ancient and historical ceramics will be traced using ceramic phase diagrams, *i.e.* chemographical expressions of Goldschmidt's mineralogical phase rule. In particular, the systems $CaO-Al_2O_3-SiO_2$

DOI: 10.1180/EMU-notes.20.6

(in which most ancient low- to medium-fired ceramics can be accommodated), $K_2O-Al_2O_3-SiO_2$ (applicable to high-fired Chinese stoneware and European hard-paste porcelain) and $Na_2O-CaO-(Al_2O_3)-SiO_2$ (typical of some ancient Egyptian and Mesopotamian alkaline glazes and French soft-paste porcelain) are discussed.

1. Introduction

The dawn of ceramic technology is irretrivably lost in the distant past, concealed from us by the impenetrable veil of ignorance and time. The history of ceramics as part of every-day life of man presumably had its origin at a time when late Neolithic hunter-gatherer bands turned into agrarian societies, some 12,000 years ago. There is, however, growing evidence that much earlier some Late Palaeolithic or Early Mesolithic genius observed that a soft clay lump would harden in a campfire, and may have realised that this novel property could be exploited to fashion cooking pots and storage containers to hold liquids.

During the past decades, our knowledge of the origin of ceramics technology has been pushed back by archaeological research well into the Upper Palaeolithic/Mesolithic period. Arguably, among the first objects fashioned from clay were maternal goddess images such as the famous Upper Palaeolithic 'Venus of Dolni Věstonice', Moravia, and fragments of animal and human figurines dating around 28,000 BP (Klima, 1962). Close to the end of the Mesolithic period (13,000–12,000 BP), hunter-gatherer communities who roamed what today is Japan, discovered ceramic technology independently (Nakamura *et al*., 2001), but this time applied it to manufacture the rope-patterned ceramic vessels of the Jōmōn culture, among the world's oldest pots (Chard, 1974; Klein, 1980). Very recently, in a cave in southern China even earlier remains of ceramic technology became known, dated to between 18,300 and 15,430 cal BP (cal BP = calibrated date before present) (Boaretto *et al*., 2009). In the African realm, pottery appeared in sub-Saharan West Africa (Mali) as early as in the middle of the tenth millennium cal BCE (cal BCE = calibrated date before the common era) (Huysecom *et al*., 2009). Because ceramic shards are generally well preserved in all but the most acidic soils they are of overriding importance to archaeology to date and distinguish prehistoric cultures by the unique and enduring physical and stylistic features of their characteristic pottery.

There is a close relationship between technological progress, and life and work organization within a society (Heimann, 1991). The evolution of ceramic technology commonly reflects this interdependent relationship. Roman Terra Sigillata, for example, was a ceramic product highly cherished because of its consistent properties, durability, easy availability, practicality, and artistic expression. Hence, many consider this medium–high-fired earthenware the 'Meissen' ware of its time. At this point, it may be appropriate to reflect on ceramic technology progress in general, and to classify any technological development by two descriptive terms: holistic and prescriptive. 'Holistic technologies' are associated essentially with crafts and artistry, prescriptive ones with industry. During much of its history, the process of making pottery was, with a few notable exceptions, a typical holistic process involving a single, stepwise approximation towards the final object whereby the potter, starting with a conscious selection of appropriate raw materials, was required to master the whole succession of

steps to produce the pot. In contrast to this, 'prescriptive technologies' involve the division of labour whereby the total work process is subdivided into rather simple unit-procedural steps that represent autonomous skills and thus draw on different groups of workers. Consequently, a considerable degree of abstraction and a solid technical understanding are necessary to integrate the individual unit processes by appropriate measures of work organization and control. The making of Roman Terra Sigillata constitutes an important early pre-industrial example of this tendency, during which labour was organized and subdivided (Roberts, 1997): different groups of workers mined clay, prepared the ceramic masses, made moulds, formed the vessels using these moulds, gathered fire wood, stoked the kilns, inspected, sorted, crated and shipped the finished pots.

The invention of ceramics was an immensely important and far-reaching paradigmatic shift in human evolution. It was the first conscious attempt of humans to alter their given natural material environment. This attempt provides a prime example of a trend observed generally in technology development. At the formative stage of any society, all the utilized technology is holistic. Only after accumulation of extensive practical knowledge and theoretical understanding, can generalization and abstraction occur. Only then can a prescriptive process emerge that in time achieves the necessary level of standardization and organization (Franklin, 1980). In this regard, the production of Roman Terra Sigillata was an important turning point in ceramic development as the holistic process of making pottery was replaced by a novel prescriptive technology that relied on process-determined division of labour, using the combined skills of many individuals. It should be emphasized that the presence and utilization of machinery is not a prerequisite for this development. Instead, the essential characteristics and indispensable requirement for a prescriptive process is 'control' that includes being in command of material resources including capital, information and people. Information includes not only technical knowledge but also the tools of control such as regulations, co-ordination, supervision, and not least, enforcement.

As will be described below in detail, clay-based ceramics are the result of an attempt to turn weathered remnants of rock back into artificial rock-like products by the action of heat on earthy raw materials (Heimann and Franklin, 1979; Cultrone *et al*., 2001; Maggetti, 2001). This development was thought to have been triggered by the Neolithic transition from hunter-gatherer to agrarian societies, a long-championed but actually outdated view (Jordan and Zvelebil, 2009). Indeed, the manufacturing of pottery typically implies some form of sedentary lifestyle, because pottery is inherently breakable and thus generally useless to hunter-gatherers who are constantly on the move. Firing of clay results in a product with a mineralogical composition different from that of the original natural material. All thermal reactions that transform the raw clay material into the final ceramic object proceed towards some equilibrium state. True thermodynamic equilibrium, however, will never be completely attained because of the relatively low firing temperature and the short firing time applied by the potter. Consequently, we have to focus our attention on the kinetics, *i.e*. the dynamic nature of the firing process. Much research in the field has shown that a fired ceramic body is

characterized by 'frozen-in' and thus aborted phase transitions that deviate strongly from true, *i.e.* thermodynamic equilibrium. However, this non-equilibrium state provides the ceramic analyst with important clues as to how, when and where the object under investigation was produced (Heimann, 1982).

Modelling the composition of fired ceramics requires the use of standards based on the expected equilibrium composition, if the limiting factors imposed by reaction kinetics are taken into account. Thermodynamics, as important a guidepost as it may be, can tell only which reactions among the minerals in a clay are allowed to occur at a given temperature and kiln atmosphere. Kinetics, however, constrains the thermodynamic 'licence' to proceed towards equilibrium by retarding reaction rates because of low temperatures, large temperature gradients in primitive pottery kilns, short reaction times, non-uniform grain-size distributions, inhomogeneously distributed reaction partners and varying redox conditions. Thermodynamics will thus control the reactions at higher temperatures and for longer reaction times under equilibrium conditions whereas kinetics will exercise control at lower temperatures and for shorter times, resulting in non-equilibrium states.

Chemically speaking, nearly all ancient low- to medium-fired earthenware can be contained in the component space of the ternary oxide system $CaO-Al_2O_3-SiO_2$. High-fired stoneware and porcelains can be accommodated in the ternary oxide system $K_2O-Al_2O_3-SiO_2$. Iron oxide, magnesia and other elements are always present in smaller quantities, and can generally be summed with geochemically similar elements. Whereas this suggests high chemical complexity, the number of phases formed during firing is surprisingly small, and their stoichiometry is comparatively simple. Condensed three-component phase diagrams, therefore, are invaluable sources of information, even though they have been derived under equilibrium conditions. Knowledge of the ceramic phase diagrams provides the key to understand, on the one hand, the relations between mineralogical and chemical composition of the precursor clays, the maximum firing temperature reached, and the firing atmosphere utilized. On the other hand, important information can be obtained about the firing time, and the microstructure, fabric, colour and eventually the mechanical and thermal properties of the ceramic product under investigation (Heimann, 1989).

2. Ceramic phase diagrams

2.1. Derivation of phase diagrams

In mineralogy and materials science, it is an established procedure to express the composition of an assembly of different phases using a 'phase diagram'. Depending on the number of components present, there exist unary, binary, ternary and multinary phase diagrams. Although a natural clay contains many oxide components owing to its complex mineralogical composition, the following brief discussion of phase diagrams will be limited to binary and ternary cases.

Phase diagrams are chemographical representations of the famous Gibbs' phase rule (Gibbs, 1878) that relates the number of phases *[Ph]*, the number of components *C*, and

the number of degrees of freedom *df* of a (closed) system by the deceptively simple equation

$$[Ph] + df = C + 2 \quad (1)$$

Components are defined as those simple oxides that combine to constitute the phases present at equilibrium, *i.e.* those portions of a system that are physically homogeneous and mechanically separable. The number of degrees of freedom is the number of variables that can be altered without changing the number of phases present. The number '2' in equation 1 is applicable when both temperature and pressure have to be considered. In systems of importance for ceramics, however, the vapour pressure is very low over a wide range of temperatures. The pressure variable can thus be ignored safely. Such systems with a reduced degree of freedom are called 'condensed' systems, and equation 1 reduces to

$$[Ph] + df = C + 1 \quad (2)$$

This equation is also called the 'mineralogical phase rule' (Goldschmidt, 1911). Systems with $C = 2$ are known as binary systems, *e.g.* $Al_2O_3-SiO_2$, systems with $C = 3$ are known as ternary systems, *e.g.* $CaO-Al_2O_3-SiO_2$. In the remainder of the current chapter, (crystalline) mineral phases, *[Ph]*, will be denoted by square brackets to distinguish them from components, *C*. This is done to avoid confusion between components and phases.

2.1.1. Binary systems

Instead of oxide components such as CaO and SiO_2, mineral phases or other chemical molecules and compounds can be displayed in binary or ternary phase diagrams. Figure 1a shows the simple binary system anorthite–diopside at ambient pressure. This particular system plays a crucial role in describing the composition and texture of basaltic rocks, *i.e.* of effusive igneous rocks with 45–52 wt.% SiO_2 (Fig. 2). The composition is given on the abscissa, and the percentage of diopside increases towards the right. The ordinate depicts the temperature; the melting points of the pure compounds are 1550ºC (anorthite) and 1390ºC (diopside), respectively. With increasing admixture of diopside to anorthite, and anorthite to diopside, respectively, the melting point of the mixture decreases according to Raoult-van't Hoff's law that describes quantitatively the melting point depression of each end-member composition as

$$\Delta T = \frac{RT_A^2}{\Delta H_f} \cdot x_B \quad (3)$$

whereby ΔT = change in melting temperature, T_A = the melting point of pure component A, x_B = mole fraction of B in the melt, R = the universal gas constant and ΔH_f = molar heat of fusion (Wachtman, 1969).

The melting points for all anorthite–diopside ratios lie on the so-called liquidus curves that intersect at the eutectic point e_{An-Di}. At any point along the liquidus curves two phases exist: either solid anorthite + melt or solid diopside + melt. Consequently, the degree of freedom (*df*) of the system is one, *i.e.* one variable: either the composition or the temperature can be varied without changing the number of phases *[Ph]* = 2, to

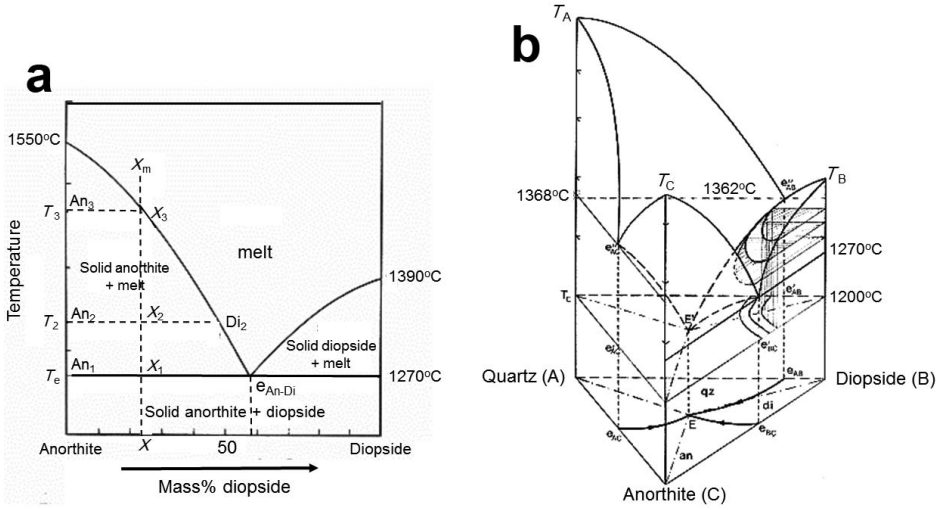

Figure 1. (a) Binary phase diagram anorthite–diopside without intermediate compound or solid solution (after Bowen, 1915). (b) Ternary phase diagram anorthite–diopside–quartz (after Clark *et al*., 1962; Osborn and Tait, 1952), showing (i) the complex curved liquidus surface (top), (ii) the planar isothermal solidus surfaces (middle) tangent to the ternary eutectic point E′ at 1200ºC, and (iii) the planar subsolidus surface (bottom) at ambient temperature. The binary eutectics at 1362ºC (quartz–diopside), 1368ºC (quartz–anorthite) and 1270ºC (anorthite–diopside) are also shown. On the right, as an example, isotherms have been projected downwards from the liquidus surface onto the solidus surface. Both images were taken from Heimann (1989).

fulfill equation 2 for this univariant equilibrium. At the eutectic point (from Greek: *eu* easy, well; *tektein* to melt) e_{An-Di} at 1270ºC, the two solid phases anorthite and diopside are in equilibrium with the melt. Hence, the number of coexisting phases, *[Ph]* is three, and $df = 0$ as any change of temperature or composition will displace the system from point e_{An-Di}. This is called an invariant equilibrium.

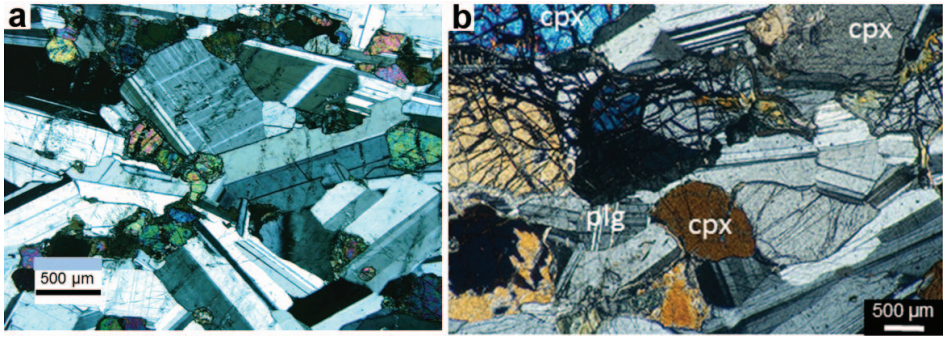

Figure 2. (a) Thin section of diabase with porphyritic or interstitial texture. (b) Thin section of gabbro with ophitic texture, showing large crystals of clinopyroxene (cpx) next to plagioclase (plg). Images by David Walker (http://microscopy-uk.org.uk).

The construction of phase diagrams usually starts from a homogeneous melt, *i.e.* at a temperature well above the liquidus. During cooling of this melt, the onset of crystallization is observed and the corresponding temperatures recorded. In the binary anorthite–diopside system, the overall composition of the melt X_m may be 77 mass% anorthite, 23 mass% diopside and is represented by an isopleth, the vertical dashed line in Fig. 1b. At the starting point X_m, above temperature T_3, the melt starts to cool. At X_3, the temperature of the melt equals T_3. A small amount of solid anorthite appears because the melt composition has now reached the liquidus curve. On further cooling, anorthite will continue to solidify while the composition of the remaining melt in equilibrium with solid anorthite follows the curve X_3–e_{An-Di} moving towards smaller amounts of the anorthite component because solid anorthite is being removed by solidification.

The amount of melt coexisting with solid anorthite at each temperature can be estimated by applying the so-called lever rule (Fig. 1a). For example, at the temperature T_2 solid anorthite An_2 is in equilibrium with a melt of composition Di_2 (52 mass% anorthite, 48 mass% diopside) in the ratio of the line lengths $X_2Di_2/An_2X_2 = 0.92$. Further cooling results in solidification of still more anorthite until at the eutectic temperature, T_e, the eutectic point, e_{An-Di} is reached. At this point (42 mass% anorthite, 58 mass% diopside) the temperature will remain constant owing to the release of the latent heat of crystallization, until all traces of melt have solidified into a mixture of solid anorthite and solid diopside. Frequently, a typical eutectic microstructure develops that is commonly lamellar (layered) due to the reduced diffusion distances in the solid state.

Whereas the size and the shape of the crystals formed during cooling of a melt depend heavily on the rate of cooling, their compositions depend on where the starting melt composition is located in the phase diagram with respect to the eutectic point. If the starting composition of the melt (X_m) is to the left of the eutectic point (hypoeutectic) (Fig. 1a), the first phase to appear during cooling is anorthite. As shown in Fig. 2a, large crystals of anorthitic plagioclase dominate the microstructure of typical porphyritic basalts. Plagioclase crystals continue to crystallize until at the eutectic temperature the remaining melt solidifies, forming a fine-grained aggregate of pyroxene + anorthite that fills the interstitial spaces among plagioclase crystals. In contrast, when starting from a melt composition to the right of the eutectic point (hypereutectic), pyroxene is first to crystallize in large crystals until on reaching the eutectic temperature a fine-grained mixture of pyroxene and plagioclase crystallizes. Such so-called ophitic texture is characteristic for gabbros, *i.e.* intrusive igneous rocks with 45–52 wt.% SiO_2, a typical composition of clinopyroxene and plagioclase, with minor contributions of olivine and amphibole (Fig. 2b).

Whereas the basaltic rocks shown in Fig. 2 appear to have crystallized under near-thermodynamic equilibrium, for ceramics the situation is strikingly different. Here the rates of heating and cooling are very fast compared to rocks such as diabase or gabbro formed from a crystallizing melt within the Earth's crust. Hence, crystals in ceramics will generally be very small, and there is frequently a large proportion of amorphous,

i.e. glassy material present. Moreover, during ceramic firing, the liquidus will not be approached by cooling a melt from high temperatures but instead by heating a solid mixture of the components. Then, in our example, a mixture of solid anorthite and diopside of composition X will lead at the temperature T_e to the formation of a partial melt of eutectic composition e_{An-Di}. According to the lever rule, the ratio of solid to melt is then $X_1e_{An-Di}/An_1X_1 = (58-23)/23 = 1.52$. With increasing temperature, the amount of melt increases until at temperature T_3 all traces of solid will have disappeared. Then the composition of the melt is X.

Because potters do not desire to melt completely the mineral mixture called clay during ceramic firing, the comparatively low firing temperatures and short firing times will never allow thermodynamic equilibrium conditions under which a ceramic phase diagram may be obtained experimentally to be reached. Hence, thermodynamics will be overruled by kinetics, and application of ceramic phase diagrams to the situation prevailing in ancient pottery kilns must abide by the constraints imposed by kinetic retardation of the potential multitude of mineral reactions as discussed above.

2.1.2. Ternary systems

Another level of complexity is attained when a third component is added to a binary phase diagram. A ternary diagram is then obtained that can be depicted in a compositional triangle (Fig. 1b, Fig. 3a). However, in this case the temperature cannot be plotted directly but can be described only by isotherms that are projections down the temperature axis perpendicular to the triangle. The liquidus surface describes the melting points of all given compositions whereby the points T_A, T_B and T_C are the melting points of the pure components A (quartz), B (diopside), and C (anorthite). If, for example, component B is added to pure A, the melting temperature of this mixture decreases along the liquidus line $T_A-e''_{AB}$. At the binary eutectic point e''_{AB}, the lowest melting temperature (1362ºC) of all compositions in the binary subsystem A–B is reached. Adding component C eventually leads to the lowest possible melting temperature, T_E, of the ternary system, the ternary eutectic point E′ at 1200ºC in the centre of the triangle A–B–C (Fig. 1b).

The second surface shown in Fig. 1b is the isothermal solidus surface tangent to the ternary eutectic point E′. This surface determines the compositions of the solid phases in equilibrium with the ternary eutectic melt. Below this surface a liquid phase cannot occur. The third surface shown is the projection of the 3D-phase diagram down to ambient temperature, the isothermal subsolidus surface A–B–C. Indicated on this surface are the stability fields of the phases [A], [B] and [C], separated by the curved phase boundary lines $e_{AC}-E$, $e_{BC}-E$ and $e_{AB}-E$, as well as the conodes A–E, B–E and C–E. In actual phase diagrams, the isotherms shown in Fig. 1b as (curved) planes parallel to the solidus surface and intersecting the liquidus surface $T_B-e''_{BC}-E'-e''_{AB}$ are projected downwards onto the solidus surface in much the same way as elevation contours on a topographical map. The 3D-ternary phase diagram shown in Fig. 1b depicts the actual system quartz (A)–diopside (B)–anorthite (C) with the melting points T_{qz} = 1723ºC, T_{di} = 1390ºC, T_{an} = 1550ºC; the binary eutectics at 1362ºC

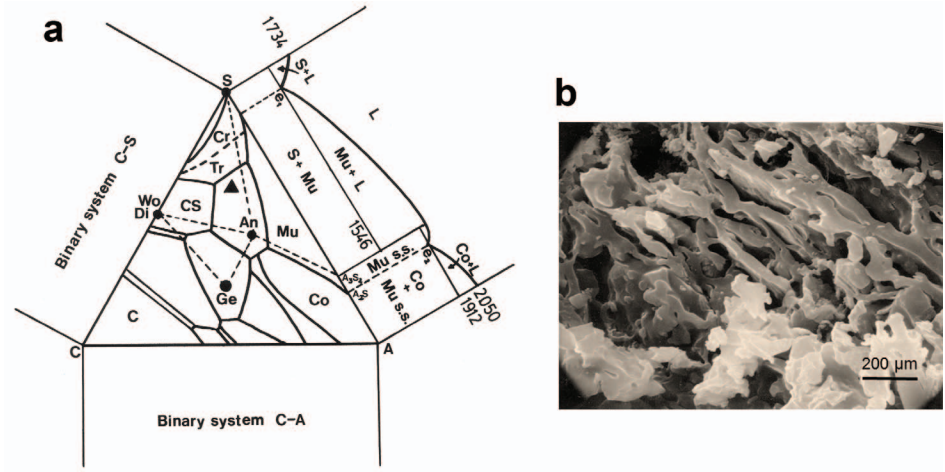

Figure 3. (a) The ternary system CaO (C)−Al_2O_3 (A)−SiO_2 (S) surrounded by the three binary systems CaO−SiO_2 (C−S, calcium silicates), CaO−Al_2O_3 (C−A, calcium aluminates) and SiO_2−Al_2O_3 (S−A). The binary system SiO_2−Al_2O_3 is shown explicitly and reveals two eutectic points, SiO_2−mullite [Mu]−liquid [L] at e_1 (T_e = 1546ºC) and mullite−corundum [Co]−liquid at e_2 (T_e = 1912ºC). Within the triangle depicting the ternary system, the phases have been denoted as follows: An: anorthite, C: calcium oxide, Co: corundum, Cr: cristobalite, CS: (Wo) wollastonite, Ge: gehlenite, Mu: mullite, and Tr: tridymite. Thick lines denote phase boundaries; dashed lines are representative of compatibility triangles (after Rankin and Wright, 1915). (b) Calcareous illitic clay of the composition indicated by the black triangle in the ternary phase diagram, experimentally fired at 1010ºC under oxidizing conditions (Heimann *et al*., 1980). With permission by cfi Ber. DKG.

(quartz−diopside), 1270ºC (diopside−anorthite), 1368ºC (quartz−anorthite); and the ternary eutectic at 1200ºC. The composition of the ternary eutectic is 30 mass% quartz, 33 mass% diopside and 37 mass% anorthite (Osborn and Tait, 1952; Clark *et al.*, 1962). The ternary phase diagram discussed above refers to high-fired calcareous illitic clays with the four components SiO_2, Al_2O_3, CaO and MgO but fails to incorporate an important fifth component such as Fe_2O_3. Hence, even more complex phase relations have to be considered in appropriate multicomponent (multinary) systems.

Each ternary system can be deconvolved into its three constituent binary systems as shown in Fig. 3a. The binary boundary systems of the ternary system CaO (C)−Al_2O_3 (A)−SiO_2 (S) have been collapsed onto the plane of the ternary system. The black triangle in the compatibility triangle wollastonite [Wo]−anorthite [An]−silica [S] depicts the composition of a typical calcareous illitic clay reportedly used by Roman potters during the first few centuries CE to produce Terra Sigillata at *Tabernae* (today's Rheinzabern, Palatinate, Germany) (Heimann and Maggetti, 2014).

Figure 3b is a scanning electron microscopy image of this calcareous illitic clay, with a chemical composition shown in Table 1, which was fired in air at 1010ºC. Intensive vitrification is apparent (Maniatis and Tite, 1975). The fabric of the pottery has been dissolved into sheets of vitrified material that are arranged parallel to the direction of compression during extrusive forming or throwing on a potter's wheel. X-ray

diffraction analysis (Heimann *et al.*, 1980) revealed that crystalline quartz, anorthite-rich plagioclase and diopside are the main constituents. This is exactly the equilibrium composition to be expected from the location of the clay composition in the compatibility triangle [silica = quartz]–[anorthite]–[diopside] shown in Fig. 3a. Minor amounts of hematite and sanidine (high-temperature alkali feldspar) account for the iron and alkali contents, respectively, of the raw clay.

In Fig. 3a the conode or tie line connecting the compositions of the conjugate phases wollastonite [Wo] and anorthite [An] (dashed line) is partitioned by the intersection with the phase boundary CS [calcium silicate]–An [anorthite], approximately in the ratio Wo/An = 58/42, corresponding to the position of the eutectic point shown in Fig. 1a. The formation of diopside would be expected because the starting clays contain 2.7 mass% MgO. However, the representation of [Di] as an individual phase would require a quaternary phase diagram that cannot be rendered in two dimensions.

The discussion above of the construction, evaluation and interpretation of binary and ternary phase diagrams considered only very simple and hence, straightforward cases. Situations in reality are more complex, involving formation of multinary compounds from the melt, occurrence of miscibility gaps among solid solutions, spinodal demixing, peritectic systems with incongruent melting, solid solutions, redox equilibria, construction of crystallization paths during freezing of a melt, and liquid immiscibility conditions. To obtain information on these peculiarities, the reader is referred to the pertinent literature (see Levin *et al*., 1964–1990; Kingery *et al*., 1976; Rosenberger, 1979; West, 1982; The American Ceramic Society, 1992–1996; Heimann, 2010). With the advent of modern high-speed computers, a vast number of software programs and thermodynamic modelling approaches is available, sometimes as freeware distributed *via* the internet (Schultz and Chang, 1985; Andersen *et al.*, 1993; Chatterjee *et al.*, 1998). Kattner (1997) provided a useful guide to these programs and their capabilities. Older but pedagogically excellent information on the laws of stability and coexistence of minerals including application of Schreinemaker analysis to multicomponent systems of geological relevance can be obtained from Niggli (1954).

2.2. Micro- or local equilibria

In contrast to the straightforward cases discussed above in which global equilibrium is regarded as extending over the entire spatial dimension of the system, the concept of micro- or local equilibria applies to ceramic systems under generally non-equilibrium conditions. These local equilibria are established whenever individual mineral grains are in close contact with each other. Their differing chemical potentials, μ_i, will become the driving force for heterogeneous mineral reactions that will approach, but never completely reach, chemical equilibrium. Ideally, these mineral reactions will proceed until thermodynamic equilibrium has been attained, defined by $dG = 0 = -s \cdot dT + \Sigma \mu_i dn_i$, whereby s is the molar entropy, μ_i the chemical potentials of components i, and n_i are the mole numbers (concentrations) of the components i.

The firing process to which clays are subjected results in a distinct state of sintering, dependent on firing temperature, firing time, composition of the raw material and kiln

atmosphere. It can be expected, therefore, that the relationship between chemical and mechanical properties of the ceramic product and the multitude of predictor variables is exceptionally complex, and in many cases impossible to unravel. Fortunately, there are several ways to overcome this problem. One involves retrospective estimation of firing conditions by assessing temperature-dependent properties of the particular clay. Thus, the properties of the ceramic body, such as phase content, colour, density, hardness, strength, toughness and magnetic properties will be compared to those of a series of similar or, ideally, identical clays fired at various temperatures under controlled conditions in the laboratory. These series form a system of reference samples with a characteristic, temperature-dependent mineralogical phase composition against which the composition of the actual ceramics can be matched (Heimann and Franklin, 1979). Analytical tools to determine the mineralogical phase composition are X-ray diffraction (XRD), optical and electron microscopy, vibrational spectroscopy such as infrared (IR) or Raman, and a host of other modern surface analytical techniques (see, for example, Kingery and Vandiver, 1986; Kockelmann *et al*., 2001).

Because the firing of a ceramic body is a short-term event, the time during which the object was subjected to the maximum firing temperature is rarely sufficient to attain a global equilibrium situation ($dG = 0$) with respect to the phase transitions initiated by the thermal treatment. In particular, a calcareous clay fired for only a few minutes to a maximum temperature below 800–850ºC in a typical bonfire retains its calcite content completely even though the thermodynamic decomposition temperature of calcite has been exceeded (Maggetti *et al*., 2011). This again witnesses how kinetic constraints override thermodynamic laws.

Likewise, kinetic retardation must be taken into account in thermal decomposition reactions of primary clay minerals such as illite or kaolinite, and non-plastic minerals such as quartz as well as the formation of high-temperature minerals such as gehlenite, diopside or mullite. As discussed above, the ceramic phase diagrams generally have been constructed from information gathered during slow cooling of silicate melts, in which the formation of new phases from the melt is accelerated because the mass-transfer coefficients are much larger in a liquid than in a solid. In fired clays, however, the temperature is usually not sufficiently high to melt the raw material completely and is not desired either. Even if partially melted phases existed in the ceramic body as in high-fired stoneware or porcelain, or in the low-to medium-fired slips of Mesopotamian Tell Halaf and Cretan Kamares wares or Roman Terra Sigillata, the considerable viscosity of these silica-rich melts largely prevented the crystallization of equilibrium phases. Hence, the state of the slips remains more or less glassy.

The ceramic body, therefore, is left in a state of distinct non-equilibrium. At lower firing temperatures, it is composed of a succession of micro- or local equilibria that are confined to the reactive interfaces between mineral grains in an inhomogeneous clay matrix (Maggetti, 1986). This situation is demonstrated in Fig. 4. On the left an aggregate of two calcite crystals, one quartz grain and one illite flake is shown schematically. The five existing microequilibria are denoted 1 to 5, and their loci in the

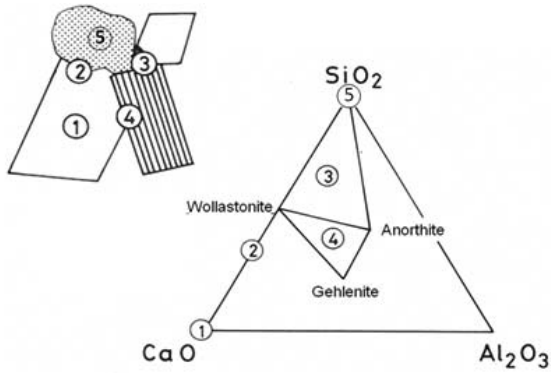

Figure 4. Schematic representation of microequilibria in a typical calcareous clay fired under oxidizing conditions (Maggetti, 1986). Left: white = calcite, stippled = quartz, laminated = illite. Right: Location of typical microequilibria 1 to 5 in the ternary phase diagram $CaO-Al_2O_3-SiO_2$. For explanation, see text.

ternary phase diagram $CaO-Al_2O_3-SiO_2$ are shown on the right. This diagram is particularly important for the calcareous illitic clays widely used by potters in antiquity, and hence is discussed in more detail here. Calcite converts on heating to CaO, and thus obtains position 1 at the CaO apex of the phase diagram. At the boundary between calcite and quartz crystals, two compatible phases of the binary subsystem $CaO-SiO_2$ form, for example, wollastonite, $Ca_3(Si_3O_9)$ and rankinite, $Ca_3Si_2O_7$. The approximate positions of the contact zones are indicated at 2. The microequilibrium 3 is stable at the three-grain boundary quartz–calcite–illite, and the position of the reaction product is somewhere in the subsystem wollastonite–anorthite–quartz, depending on the relative proportion of the components: the exact position depends on the relative proportions of the original minerals. Microequilibrium 4 between calcite and illite contains less SiO_2 component than microequilibrium 3, and is therefore located somewhere in the subsystem wollastonite–anorthite–gehlenite. Finally, the quartz will be located at the SiO_2 apex 5.

The existence of microequilibria gives the ceramic analyst an important tool at hand to perform mineralogical analyses of grain-boundary melts, reaction rims and pores using optical and electron-optical techniques (Heimann *et al*., 1980). The results obtained often lead to sound conclusions about the crystallization paths towards equilibrium (see Section 4.3.4.).

In conclusion, the useful concept of microequilibrium explains why thermodynamically incompatible mineral phases such as gehlenite and quartz can occur side-by-side in the ceramic body obtained from a calcareous paste. This is caused by the inherent inhomogeneity (graininess) of the clay, and the low temperatures and short firing times applied during firing. These conditions are not sufficient to attain thermodynamic equilibrium with respect to the global system. This situation reflects again the universal struggle between thermodynamic and kinetic principles in that there exists the thermodynamic ‘license’ to proceed with a certain phase-transformation reaction, but the low maximum firing temperature, steep heating rate and short reaction time impose a

kinetic constraint resulting in retarding the expected reactions. Thermodynamics will control the reactions at high temperatures and for long reaction times; kinetics will exercise control at lower temperatures and shorter times. This occurs because large amounts of activation energy and configurational entropy, $-s \cdot dT$, respectively are required to nucleate a new phase. Because these driving forces are not available at the relatively low temperatures employed by an ancient potter, metastable 'frozen-in' equilibria dominate the ceramic microstructure as evidenced, for example, in Neolithic ware.

In any case, the formation of gehlenite from calcareous clays by grain-boundary reactions (Maggetti and Heimann, 1979) is surprising because, from a thermodynamical point of view, the formation of an Al-rich pyroxene such as fassaite, $Ca(Mg,Al,Fe^{3+})(Si,Al)_2O_6$ (Tilley, 1938) would be expected (Dondi *et al*., 1998; Cultrone *et al*., 2001). However, in this case another example of kinetics overriding thermodynamics is brought to bear because, according to Goldsmith's 'ease of crystallization' principle (Goldsmith, 1953), a silicate phase with Al only in fourfold coordination is energetically favoured over phases containing Al in mixed four- and sixfold coordinations, at least in the absence of hydroxyl ions. Because in the crystal structure of gehlenite all Al ions are in tetrahedral coordination (Louisnathan, 1971), this phase will form preferentially. Similarly, the preferential formation of mullite with a larger $(AlO_4)/(AlO_6)$ ratio than structurally similar sillimanite (Rehak *et al*., 1998) could be explained by Goldsmith's rule.

3. Oxidizing *vs*. reducing firing – the role of the oxygen partial pressure

Figure 5 summarizes the disappearance of several typical minerals that make up calcareous illitic clay and the appearance of new phases that occur under oxidizing (left) and reducing (right) conditions. The phases were identified by XRD.

The onset of formation of diopside and/or gehlenite in oxidizing fired calcareous illitic clays at ~800ºC leads to a profound change in the fabric of the ceramic body as

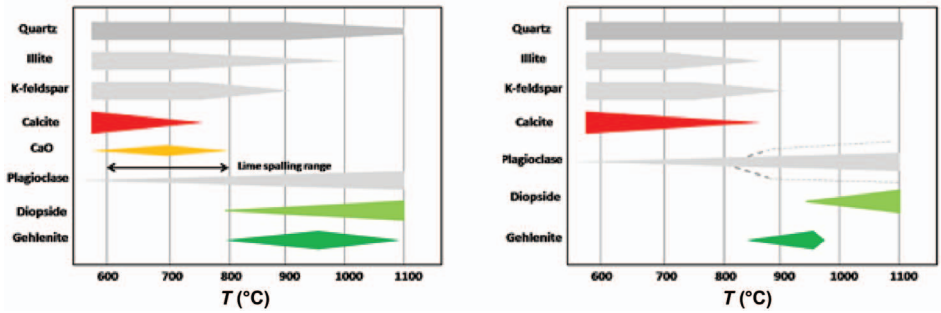

Figure 5. Experimentally determined phase stability in calcareous illitic clay fired under oxidizing (left) (Maggetti, 1982) and reducing (right) (Letsch and Noll, 1983) conditions. Under oxidizing conditions, illite is found to be stable to higher temperatures while decarbonization of calcite is impeded under reducing conditions. Onset of formation of diopside occurs at a lower temperature in the presence of high oxygen partial pressure.

partial melts are formed, the amount of which increases with increasing firing temperature. In contrast to this, calcareous ceramics that do not contain diopside are thought to be fired much below 800ºC, typical of the overwhelming majority of Neolithic pottery. In this case, the thermal decomposition of calcite, which starts at 600ºC and finishes at ~850ºC, is not completed yet (Rodriguez-Navarro *et al*., 2009) or these wares were fired for only very short times that were insufficient to decompose larger calcite grains into reactive CaO that would give rise to diopside and gehlenite formation (Maggetti *et al.*, 2011). Nevertheless, the occurrence of diopside can, with caution, be considered an important indicator of the (maximum) firing temperature attained, and thus is at least a rudimentary marker of the technological skill of the potter. The same clay fired under reducing conditions shows a delayed onset of both diopside and gehlenite formation owing to the fact that the stability of calcite is extended by at least 100ºC under reducing conditions, *i.e*. in the presence of CO_2 in the kiln atmosphere formed by the water–gas equilibrium $CO + H_2O \leftrightarrow CO_2 + H_2$ (Escardino *et al*., 2006). In contrast, phase evolution studies on Mg-rich calcareous illitic archaeological (?) clays from Troy, Turkey, fired under reducing conditions revealed that the onset of formation of the Mg-rich phase åkermanite ($Ca_2MgSi_2O_7$) instead of the Al-rich phase gehlenite ($Ca_2Al[AlSiO_7]$) occurs at ~750ºC, together with anorthite and sanidine, whereas diopside starts to form only at temperatures ~850ºC, *i.e.* ~100ºC lower as indicated in Fig. 5 (right) (Görres *et al*., 2000). These results were inferred from high-resolution Rietveld refinement corroborated by transmission electron microscopy (TEM), a technique capable of detecting those minute mineral neoformations that elude detection by XRD. These results show the importance of considering the chemical composition of the clays, the firing atmosphere as well as the technique employed, if determination of ancient firing temperatures is the goal. Unfortunately, studies employing such advanced analytical techniques to solve technological riddles of the ceramic past are rare.

Gehlenite formed during ceramic firing at 800−850ºC (Fig. 5, left) is metastable and reacts at higher temperatures (>1050ºC) with silica released during decomposition of metakaolinite or illite to anorthite + wollastonite (or in the presence of MgO to diopside, $CaMgSi_2O_6$) according to

$$Ca_2Al[AlSiO_7] + 2\ SiO_2 \rightarrow CaAl_2Si_2O_8 + CaSiO_3 \qquad (4)$$

The so-called ‘gehlenite problem’ is another example of the intricate interplay between thermodynamic principles and kinetic reality. The formation of gehlenite outside its field of thermodynamic stability, and its occurrence in and disappearance from calcareous illitic clays has long been considered an analytical challenge as a thermodynamic problem (Heimann and Franklin, 1979). However, the solution to this problem has been found in the realm of reaction kinetics. Roman Terra Sigillata, produced in Switzerland, does not show gehlenite, whereas Terra Helvetica, a specific Swiss subtype of the former, contains significant amounts of this mineral (Maggetti and Küpfer, 1978; Maggetti and Heimann, 1979). Because both wares were produced from similar clays and fired in the stability range of gehlenite (Fig. 5, left), it has to be assumed that well processed clays with a narrow and small grain-size distribution and,

in particular, absence of larger calcite grains, were utilized to make Terra Sigillata, whereas Terra Helvetica was made from less-processed clays with coarser calcite grains. Evidently, the reaction rate of gehlenite formation is a function of the primary calcite grain sizes which, in turn, are influenced by the degree of processing of the clay; a clear measure of the technical skill of the potter.

The mineralogical changes of a non-calcareous iron-rich illitic clay under oxidizing (top, dark bars) and reducing (bottom, light bars) conditions are shown in Fig. 6a. The main differences lie in the extended stability range of illite to somewhat higher temperatures and the earlier onset of mullite formation under oxidizing conditions. Because in contrast to calcareous clays, reaction products, *i.e.* mullite, will be formed only at much higher temperatures beyond 1000ºC, the fabric of non-calcareous clays fired below that temperature threshold corresponds, in principle, to that of low-fired calcareous clays. Hence, for firing temperatures below 1000ºC, attempts to relate the fabric of a non-calcareous ceramic body to its firing temperature are doomed in practice (Heimann and Franklin, 1979).

Varying redox conditions during the ceramic firing process account for the formation of coloured iron oxide pigments. This property provided the ancient potters with a versatile tool to adorn their objects with contrasting black and red surfaces, as shown impressively by the black-figured technique of the Corinthian potters invented around 700 BCE as well as the red-figured technique of the Attic potters discovered around 530 BCE (Heimann and Maggetti, 2014). In a pottery kiln, the prevailing redox conditions can be adjusted and manipulated *via* the Boudouard equilibrium $CO_2 + C \leftrightarrow 2CO$ that fixes the oxygen

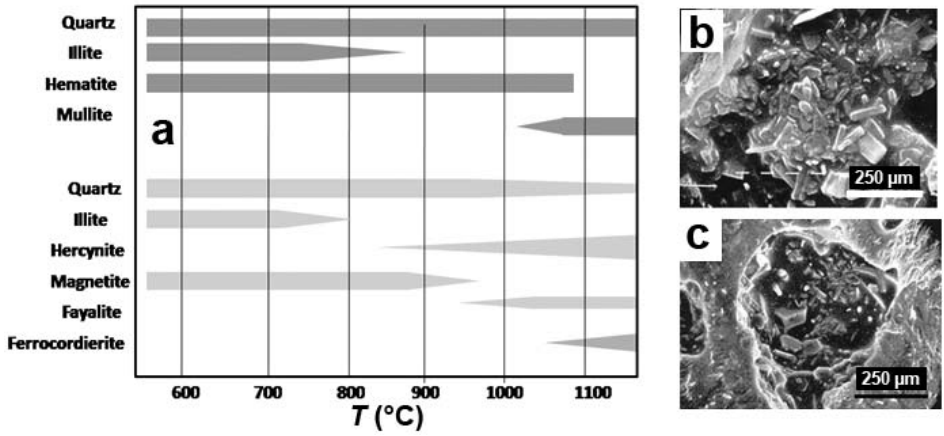

Figure 6. (a) Experimentally (XRD) determined phase stability in a non-calcareous iron-rich illitic clay under oxidizing (top) and reducing (bottom) firing conditions. Under oxidizing conditions, illite is found to be stable to somewhat higher temperatures. Onset of formation of mullite occurs at lower temperature in the presence of high oxygen partial pressure (after Heimann *et al*., 1980, Letsch and Noll, 1983). Neo-formation of anorthite-rich plagioclase (b) and ferrocordierite (c) are observed; these occur as a result of experimental firing of a non-calcareous iron-rich illitic clay under strongly reducing conditions at 1035ºC (Heimann *et al*., 1980). With permission by cfi Ber. DKG.

fugacity in such a way that ferric ions (Fe^{3+}) in red hematite are reduced to a spinel-type phase (magnetite, black) containing ferrous ions (Fe^{2+}). However, the system follows the Boudouard equilibrium only if airtight conditions prevail and gas-free fuels such as charcoal or coke are used, conditions that were never fully realized in ancient pottery kilns (Letsch and Noll, 1983). If the clay body releases oxygen and/or carbon dioxide during firing, the Boudouard equilibrium will be disturbed briefly but restored quickly by consuming additional carbon from the fuel. Any water released reacts with carbon monoxide until the water–gas equilibrium $CO + H_2O \leftrightarrow CO_2 + H_2$ is achieved; that will be catalysed in the presence of magnetite.

Because ancient pottery kilns required frequent refuelling, opening of the stoking channel and the presence of cracks in the kiln walls allowing uncontrolled ingress of air, and other changes in the air supply further disturbed the Boudouard equilibrium and created transitional states between fully and partially oxidizing firing. As a consequence, many 'reduction-fired' ceramics not only contain spinel phases such as magnetite or hercynite but also elemental carbon as black pigment phases. A telltale sign of such uncontrolled air ingress is the notorious misfired 'red-stained' ware.

During oxidizing firing, hematite is stable throughout the entire temperature range up to 1490ºC, where it reaches its dissociation pressure of 1 bar. In a reducing atmosphere, hematite is quantitatively converted to magnetite already below ~600ºC. In fired (illitic) clays, magnetite is stable until 850–900ºC, but converts through reaction with alumina released by decomposing illite to hercynite ($FeAl_2O_4$). Further temperature increase shifts the equilibrium towards the formation of Fe_xO (wüstite) that converts to metallic iron at 730ºC. Furthermore, the formation of fayalite (Fe_2SiO_4) under ideal thermodynamically controlled conditions ought to commence at 350ºC. However, at this low temperature fayalite formation is kinetically constrained by the lack of reactive silica that will be available only at much higher temperatures through decomposition of the clay minerals. Consequently, fayalite may occur in measurable amounts only in ceramics fired under reducing conditions to at least 950ºC as shown in Fig. 6a.

A useful tool to assess the degree of reduction obtained in ancient pottery kilns has been found in determining the magnetic (mass) susceptibility, χ, of fired clay. This physical property is a dimensionless proportionality constant that indicates the degree of magnetization of a material in response to an applied magnetic field. Figure 7 shows the real component of the magnetic susceptibility χ_g as a function of the firing temperature and the oxygen fugacity of the firing atmosphere of an experimentally fired calcareous illitic clay with a composition shown in Table 1. The oxygen fugacities established in an electrically heated furnace were controlled by solid-state buffer mixtures (Mn_2O_3/Mn_3O_4: weakly reducing with $f_{O_2} > 10^{-4}$ atm; Ni/NiO and Fe_2O_3/Fe_3O_4: strongly reducing with $f_{O_2} < 10^{-4}$ atm). Clay samples heated in air were used as a control ($f_{O_2} = 0.2$ atm). At a standard firing temperature of 1000ºC, the oxygen fugacities achievable with the solid-state buffers are as follows: $\log f_{O_2} = -0.56$ atm for Mn_2O_3/Mn_3O_4; $\log f_{O_2} = -5.39$ for Fe_2O_3/Fe_3O_4; and $\log f_{O_2} = -10.22$ for Ni/NiO (Huebner, 1971).

The average magnetic mass susceptibilities of iron minerals to be expected during ceramic firing increase from hematite, $(2.5–3.7)\cdot10^{-7}$ m^3/kg to fayalite,

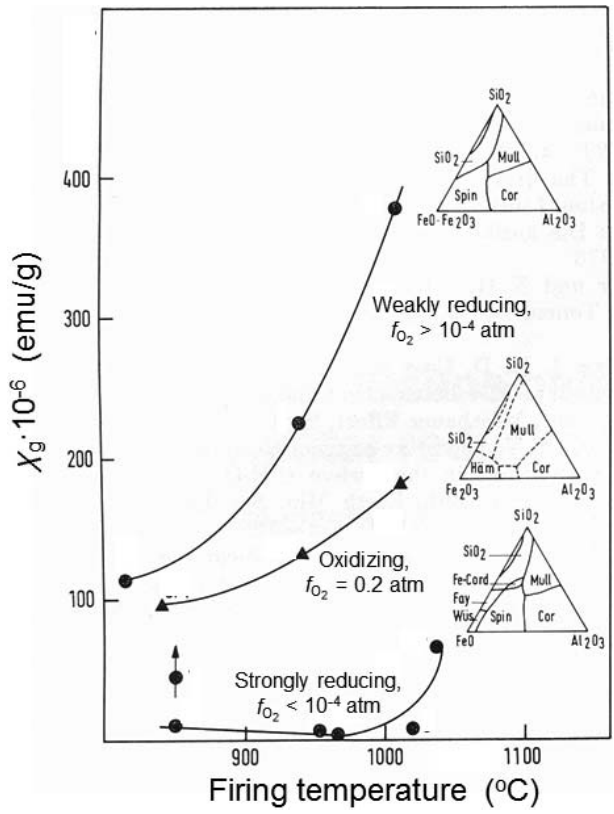

Figure. 7. Real component of the magnetic susceptibility of calcareous illitic clay fired under reducing and oxidizing conditions (Heimann *et al*., 1980). The ternary diagrams show the phases stable at the oxygen fugacities selected for the firing experiments. Cor: cordierite, Fay: fayalite, Fe-Cord: ferrocordierite, Häm: hematite, Mull: mullite, Spin: spinel (magnetite–hercynite solid solutions), Wüs: wüstite. With permission by cfi Ber. DKG.

$(0.5-13)\cdot 10^{-7}$ m^3/kg to wüstite, $(10-100)\cdot 10^{-7}$ m^3/kg to magnetite, $(2.5-8)\cdot 10^{-4}$ m^3/kg (Powell *et al*., 2002). Consequently, as is evident from Fig. 7, the magnetic susceptibilities of the samples fired under weakly reducing conditions are much greater than those of the

Table 1. Chemical composition of an archaeological clay from Otterbach, Jockgrim, Palatinate, Germany in mass% fired at 1000ºC (Heimann *et al*., 1980). With permission by cfi Ber. DKG.

SiO_2	61.7	MgO	2.7	P_2O_5	0.1
TiO_2	0.8	CaO	7.0	Ba (ppm)	514
Al_2O_3	19.3	Na_2O	0.8	Cr (ppm)	134
Fe_2O_3	5.5	K_2O	3.5	Rb (ppm)	197

samples fired under oxidizing conditions, owing to the strongly ferrimagnetic nature of magnetite. The low magnetic susceptibilities of samples fired in strongly reducing atmosphere are, at first glance, rather surprising. However, an explanation for this phenomenon can be found in the fact that the reduction of iron ions continued until all were transformed to Fe_xO. These wüstites are, in contrast to the ferrimagnetic magnetite, antiferromagnetic with a tendency to suppress the susceptibility. Hence, it causes only a weak paramagnetic response because it does not possess a spontaneous macroscopic magnetic momentum. Moreover, as Fe_xO acts as a strong mineralizer it promotes the formation of partial melts at mineral grain-boundaries from which iron aluminium silicates such as the cyclosilicate ferrocordierite (sekaninaite, $(Fe^{2+},Mg)_2Al_4Si_5O_{18}$) or the iron silicate fayalite $(Fe^{2+})_2SiO_4$ can crystallize during cooling. Indeed, the increase in the magnetic susceptibility of the strongly reduced samples beyond 1000ºC shown in Fig. 7 may be related to the formation of ferrocordierite (Heimann *et al*., 1980). It can be further surmized that a large proportion of Fe^{2+} ions generated during strongly reducing firing will remain dispersed in the glassy phase and thus cannot establish any cooperative magnetic phenomena, again accounting for the comparatively low magnetic susceptibilities measured (Fig. 7).

In summary, the onset of the formation of a partial melt phase at much lower temperature in calcareous clays compared to non-calcareous clays was the technological reason why prehistoric potters searched for clay deposits rich in calcium (and alkali) ions. Such clays could be processed easily in primitive wood-fired kilns with a bare minimum of sophistication to yield dense, mechanically durable cooking pots, bowls, strainers, plates and cups of all sorts that could well fulfil their function in the ancient kitchens and dining rooms. On the downside, highly calcareous clays have a narrow sintering interval that requires considerable temperature control (see Fig. 18). Consequently, a pronounced risk of overfiring exists as evidenced by the high proportion of misfired wasters littering ancient pottery production sites. In addition, there was always the risk of 'lime blowing', that is, spalling of the pot by rehydration of CaO to portlandite, $Ca(OH)_2$, and subsequent carbonation of this phase to re-form calcite. Hence, such calcareous clays, when used for cooking pots must be fired well below the decomposition temperature of calcite that is known to start beyond 600ºC in oxidizing atmosphere but beyond 800ºC in a reducing atmosphere (Letsch and Noll, 1983). However, these low firing temperatures lead to mechanically inferior wares. To remedy this problem, cooking pots fashioned from highly calcareous clays were frequently reinforced with coarse quartz or rock grains as temper (Kilikoglou *et al*., 1995, 1998).

Skilful manipulation of the redox equilibria of iron oxides during oxidizing and reducing firing enabled ancient potters to play with the entire colour palette from jet black to flaming red, and hence, to create aesthetically pleasing and highly treasured ceramic objects for domestic use and trade over considerable distances within the ancient world.

4. Case studies

In the following sections, we will discuss several examples of the application of ceramic phase diagrams to the technological interpretation of ancient and historical ceramics. We will proceed from low-fired pottery of old Mesopotamia, Egypt, Minoan Crete and Greece to medium high-fired earthenware such as Terra Sigillata to high-fired ceramics such as ancient Chinese and Thai stoneware, and European hard-paste and soft-paste porcelains. We have chosen this approach to show that the first group is subject to complexities introduced by kinetic constraints, whereas the second and third groups conform approximately to the thermodynamic principles developed above. Most of the information provided below has been adapted from recent work by the authors (Heimann and Maggetti, 2014). Basic references to the ceramic development and singular references to major overview publications for the period considered as well as much more information on the beauty and striking variability of ancient and historical ceramics, supported by a host of colour photographs, can be extracted from this book.

4.1. Low-fired earthenware

4.1.1. Neolithic Mesopotamian wares

Utilitarian pottery appeared around 6500 BCE in a region extending from Mesopotamia to Anatolia, the eastern arc of the Fertile Crescent. The oldest Mesopotamian wares were fired at temperatures as low as 600−700ºC as estimated for bonfired Proto-Hassuna ware. Owing to the composition of clays won from the beds of the Euphrates and Tigris rivers, the clays utilized in Mesopotamian pottery were very rich in calcium carbonate (Fig. 8). The range of fluvio-lacustrine Quaternary clay composition comprises 20−25 mass% quartz, 30−40 mass% carbonate minerals (calcite, dolomite), 30−35 mass% clay minerals, 3−6 mass% iron oxides and hydroxides, and 2−5 mass% gypsum and halite (Mustafa, 2011). The average clay content (30−35 mass%) consists approximately of 25 mass% illite, 30 mass% illite-smectite mixed-layer mineral, 20 mass% palygorskite, 15 mass% kaolinite and 10% chlorite (Kadum and Hussain, 2011). The overall chemical compositions of typical clays from the Mesopotamian plain (Nahrawan, 65 km east of Baghdad; Seleucia, 30 km south of Baghdad) are shown in Fig. 8 (open circle and star symbols).

Because the sintering temperatures of the highly calcareous illitic-smectitic clays used were <1000ºC, the resultant pottery was prone to overfiring with associate slumping owing to their small sintering interval. The composition of the calcareous river silt of Mesopotamia is in stark contrast to that of the rather lime-poor Nile silt of Egypt that dominated the composition of Egyptian ceramics independent of time and locality (Fig. 9). The low firing temperature applied to the Mesopotamian pottery rendered the ceramic body porous. This initial drawback was remedied by coating the outside of the pot with a clay slip as early as the 5th millennium BCE (Figs 8b, 10b). Soon after 2000 BCE, the Mesopotamian potters invented lead oxide glazing to render their pots impervious to water. The lead oxide glaze fused at relatively low temperature and lent itself easily to colouring with metal oxides such as copper and manganese

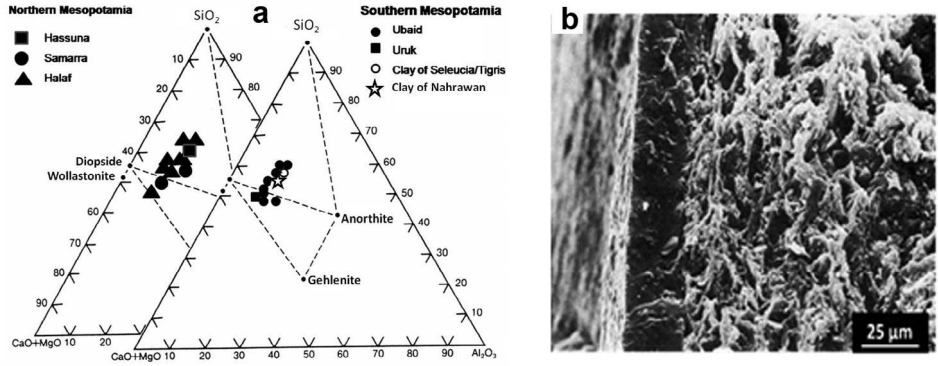

Figure 8. (a) Chemical composition of the Neolithic-Chalcolithic wares and clays from northern (Hassuna, Samarra, Halaf; left) and southern (Ubaid, Uruk; right) Mesopotamia shown in the triangle (CaO+MgO)−Al_2O_3−SiO_2. An open circle and a star (Noll, 1984, 1991; Jabbori, 1980) depict, respectively, the clays from Seleucia and Nahrawan. (b) Vitreous black engobe (left) on the porous ceramic body (right) of pottery from Tell Halaf, Mesopotamia, 5th millennium BCE (Noll and Heimann, 2016). With permission by Schweizerbart Science Publishers.

oxides, producing rich green and black colour palettes. This ingenious discovery by Mesopotamian potters led to widespread application of lead glaze that adhered particularly well to almost any fired clay surface and thus constituted an important technological advancement.

Characteristic of all locally and temporally different wares from northern (Hassuna, Samarra, Halaf) and southern (Ubaid, Uruk) Mesopotamia is their chemical

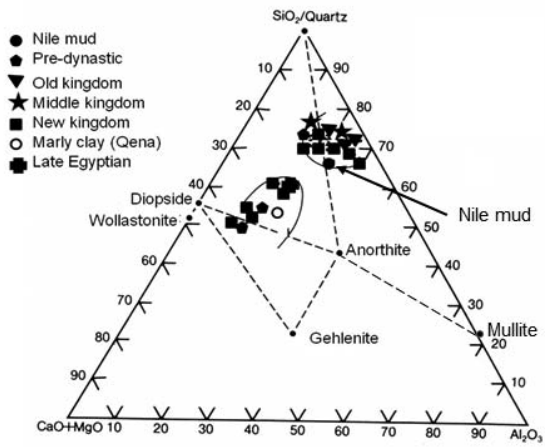

Figure 9. Composition of ancient Egyptian pottery in the ternary phase diagram (CaO+MgO)−Al_2O_3−SiO_2. Dashed lines show the three compositional triangles diopside−anorthite−quartz, diopside−anorthite−gehlenite, and quartz−anorthite−mullite (in Heimann and Maggetti, 2014). Data from Noll (1984). The composition of Nile mud was obtained from Hängst (1979).

homogeneity, owing to the homogeneity of the river-derived clay raw material. This chemical homogeneity of the ceramic body of the northern and southern Mesopotamian wares is shown in Fig. 8a. In the ternary (CaO+MgO)−Al_2O_3−SiO_2 phase diagram, the compositions of Tigris clays (open circle and star, right triangle) and the resulting ceramic wares are depicted. The clay compositions sit squarely in the compositional triangle diopside−anorthite−quartz whereas the composition of the ceramics deviates toward larger amounts of lime, presumably the result of inclusions of larger grains of calcite/dolomite in the ceramic mass owing to insufficient processing of clay that otherwise would have removed these inclusions (Noll, 1984). The content of alumina, however, is constant at ~10−12 mass% thus confirming the homogeneity of the clay source. The large CaO content of some of the ceramics shifts the phase composition into the triangle diopside−anorthite−gehlenite. Superposition of the two ternary diagrams confirms that northern and southern Mesopotamian wares are congruent, meaning that their raw materials can be traced back to the same riverine source.

Note that the ternary diagrams shown in Figs. 8 and 9 are oversimplified in that CaO and MgO were combined to only one component. Strictly speaking, two compositional triangles wollastonite–anorthite–gehlenite and diopside–anorthite–gehlenite would then exist, the first of which is not stable in the presence of larger amounts of MgO.

The history of painted ceramics produced by the iron reduction technique started with the northern Mesopotamian Hassuna and Samarra cultures in the 6th millennium BCE and reached a technologically remarkably high development stage during the Halaf period in the first half of the 5th millennium BCE (Fig. 8a, left triangle). While Proto-Hassuna ware was probably fired at a low 600−700ºC for a short time as suggested by the extent of the inner black cores of the ceramic shards, Hassuna pottery was fired at higher temperatures in updraught pottery kilns dated to the second half of the 7th millennium BCE.

Still higher temperatures estimated at between 850 and 1050ºC were attained by potters of the Samarran and Tell Halaf cultures of the first half of the 5th millennium BCE. Their kilns produced bowls and jars painted with geometric patterns in reddish-brown colours, featuring designs attesting to skilful manipulation of the valence state of iron oxides during either reducing or oxidizing firing (Fig. 10a). Halaf potters, in particular, decorated their products with a densely sintered, vitreous *engobe* (slip) that not only sealed the surface but also provided an aesthetically pleasing decorative effect (Figs 8b, 10b). This required the careful preparation of the clay suspension by efficient elutriation to obtain a homogeneous and smooth surface of the paint layer with an appealing gloss after burnishing in the leather-hard state. Despite its technological superiority, this glossy engobe technique slipped into oblivion until it was rediscovered millennia later by Middle Minoan potters who created the famous eggshell Kamares ware (Fig. 11b). From this early highlight the glossy engobe or slip technique was carried on through time: Mycenaean ware, Corinthian black-on-light and Attic red-on-black, and Roman Terra Sigillata wares all show these shiny surface layers, formed by partial vitrification during reducing (black layer) or oxidizing (red layer) firing of fine-grained, potassium- and iron-rich fusible illitic clays.

Figure 10. Iron oxide-painted earthenware pottery. (a) Samarra, Mesopotamia, 6500–6000 BCE, Reg. No. 1924,0416.8. AN 00310643.© The Trustees of the British Museum, London. (b) Ceramic cup (left) and bowl (right) from Tell Halaf with geometric cross-hatched decoration and black *engobe* around the carinated rim (6^{th}/5^{th} millennium BCE). Reg.No.VA 12468 (height 6.1 cm, diameter 8.4 cm), VA 12402 (height 8.4 cm, diameter 15.8 cm). © Staatliche Museen zu Berlin, Photo: Olaf M. Teβmer.

4.1.2. Egyptian Neolithic pottery

In Egypt, relatively lime-poor Nile silt dominated the composition of ceramics independent of time and locality. The 5^{th} millennium BCE Badarian ware is among the finest pottery ever produced in the prehistoric Near East. Their vessels excel with extreme thinness, and are well fired and highly polished. A lustrous surface gloss emphasizes the colours of black, brown and red, the latter being used frequently with a black upper body. This black colour was produced by 'smoking', *i.e.* oriented deposition of carbon flakes on the highly burnished upper rim of the so-called 'black-

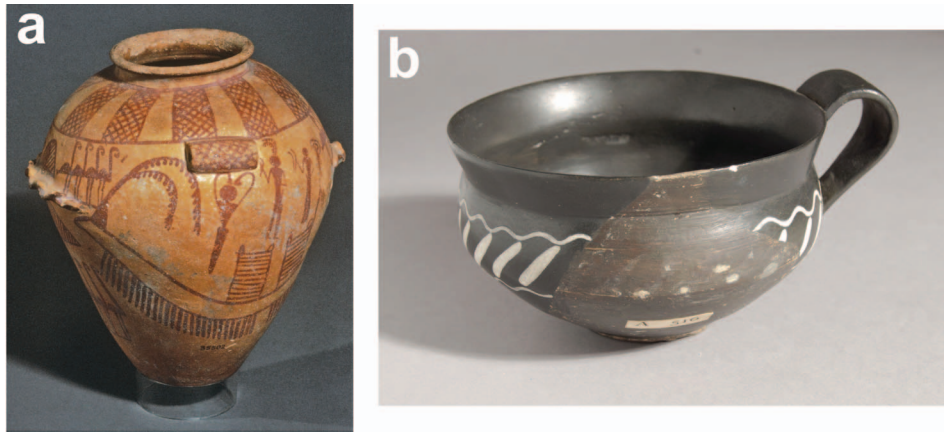

Figure 11. (a) Slip-painted earthenware jar. Naqada II period, Predynastic Egypt *ca*. 3300 BCE. Height 29.5 cm, diameter 22.5 cm. Reg.No. 1901,1012.2. AN 00076453. © The Trustees of the British Museum, London. (b) Middle Minoan IIB (1800–1700 BCE) 'egg-shell' Kamares-style cup (restored with gypsum), Height 5.7 cm. Palaiokastro, Crete. Reg.No. 1907,0119.296. AN 00756559. © The Trustees of the British Museum, London.

topped ware' (C-black technique). To add contrast, a decorative palm-leaf pattern was polished onto the air-dried clay body prior to smoking that subsequently would stand out by virtue of its silver-grey gloss over the dull black, unpolished background. This gave the vessels the appearance of high-priced and hence, prestigious metal objects.

During the Predynastic Naqada period, earthenware pottery was produced from marly clays (Noll, 1991; Noll and Heimann, 2016), slip-painted with geometric patterns as well as animal, plant and boat decorations. The Naqada I period somewhat overlapped the Badari era and eventually succeeded it with red-grounded pottery made from Nile mud, sometimes cold-painted white with gypsum. During the Naqada II stage of Predynastic Egypt, additional colours and colour combinations appeared, often disguising the red-grounded ceramic body with a light-coloured slip (Fig. 11a). This slip served as a painting ground for geometric ornaments and images of human figures and animals executed in red-brown and black colours by using iron and manganese oxide pigments instead of smoking that became a less frequently applied decoration technique.

Production of fine pottery in the Badarian tradition continued during the 3rd to 6th dynasties of the Old Kingdom (2650–2150 BCE). Red-slipped bowls of 'Meidum' type were produced from marl or silty Nile clay with a thick red slip on the interior and exterior surfaces. Such 'Meidum' bowls were highly polished and elegantly executed, with a rather large diameter, rounded bottom, and flared rim (Fig. 12b).

From a chemical point of view, all of these ceramic bodies were remarkably homogeneous, with raw clay compositions closely associated with that of lime-poor Nile silt, the composition of which is nearly constant over long distances. As shown in Fig. 9, the composition of Nile silt (normalized for loss on ignition) is ~68 mass% SiO_2, 24 mass% $Al_2O_3 + Fe_2O_3$, and 8 mass% CaO + MgO (Hängst, 1979). Hamdan *et al.* (2014) subdivided the composition of Nile silt in two types, a high-silica

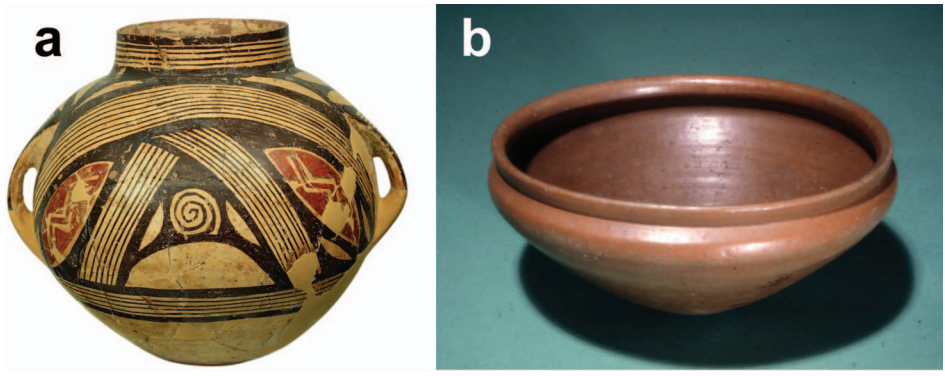

Figure 12. (a) Late Neolithic (5300–4800 BCE) spherical vase from Dimini, Thessaly. Reg. No. 5922 of the National Museum Athens, Greece. © Hellenic Ministry of Culture and Sports/Archaeological Receipts Fund. (b) Red-slipped pottery bowl of 'Meidum' type. El Badari, Upper Egypt. Old Kingdom (2650–2150 BCE). Diameter 21.6 cm. Reg. No. 1925,1012.11.AN 00424005. © The Trustees of the British Museum, London.

(~73 mass%), high-alumina (~18 mass%) and low-iron (~7 mass%) type of granitic origin (White Nile, central Africa) and a low-silica (~58 mass%), low-alumina (~11 mass%) and high-iron (~12 mass%) type of basaltic origin (Blue Nile, Ethiopia).

The composition of ceramics made from silica- and alumina-rich Nile mud straddles the tie line quartz–anorthite. Moreover, a substantial number of pottery analyses are located in the triangle quartz–anorthite–mullite, attesting to decreased CaO and increased alumina contents. However, this is not to mean that mullite had actually been formed as a firing product because the temperatures to which the clay was subjected were too low to overcome the activation energy barrier required to nucleate mullite. Indeed, the onset of mullite formation is known to require temperatures well above 1000ºC, temperatures that could be achieved only much later in improved natural or forced draught kilns.

The fact that the Nile silt composition is lowest in SiO_2 compared to the analyses of the Egyptian wares is almost certainly related to the fact that fine quartz sand was used as an intentionally added temper during production of the pottery.

The New Kingdom wares produced from very lime-rich marly clays of Qena (Dendara) and El-Ballas form a clearly separated group in Fig. 9 that extends from the low-calcareous compositional triangle diopside–quartz–anorthite to the calcareous triangle diopside–anorthite–gehlenite.

4.1.3. Aegean Neolithic pottery

Ceramics of the Neolithic sites of Thessalian Sesklo (Wijnen, 1981) and Dimini in northern Greece are two early highlights of the European ceramic development. These ceramics are considered a crucial fulcrum of the expansion of the Neolithic ceramic tradition from Anatolia to the remainder of Europe.

Close to the ancient archaeological sites Sesklo and Dimini, three types of clay occur that all were used at one time or another to produce pottery in Neolithic times (Schneider *et al*., 1990; Table 2). These raw materials comprise: (1) white illitic clays with low iron content and very poor in calcium and chromium, formed by weathering of mica schists and gneisses; (2) red tertiary clays with high iron, low calcium and relatively high chromium and nickel contents; as well as (3) alluvial clays high in chromium but with rather variable calcium contents. The composition of clay type 1 matches closely that of non-calcareous locally produced red-and-white painted pottery.

Table 2. Compositions of white illitic (1) and red tertiary (2) clays found near the Sesklo site (Schneider *et al*., 1990). Oxides are given in mass%, trace elements in ppm. Distinguishing elemental contents are shown in italics.

Type	SiO_2	TiO_2	Al_2O_3	Fe_2O_3	MnO	MgO	CaO	Na_2O	K_2O	Cr	Ni	Rb	Y
1	72.6	0.44	17.9	*2.20*	0.03	1.09	*0.54*	1.86	3.31	*51*	11	179	*13*
2	66.0	0.80	16.6	*6.54*	0.12	2.18	*1.95*	3.37	2.32	*164*	*76*	96	*51*

Various pottery styles could be distinguished from each other by their different calcium, chromium and yttrium contents (Heimann and Maggetti, 2014). Chromium contents are probably related to the presence of the mineral serpentine which is typical of ophiolitic rocks that are common throughout the mountains surrounding the Thessalian plains to the east, south and west. Only the northern parts of the plains, covered by Pleistocene terraces, yield clays that are low in chromium but have differing yttrium contents. Hence, coarse ceramic ware of the Tsangli-Larissa phase (Dimini I) found in the north could be subdivided by their yttrium content. The differences in the yttrium content of the local clays and the pottery excavated are thought to be related to geochemical differences in the metamorphic rocks located nearby. Likewise, clays and pottery from the northern site of Soufli are low in yttrium but rich in chromium (>250 ppm), a fact that attests to the alluvial nature of the clay type 3, being derived from the mountains to the east and west.

The Late Neolithic painted Classic Dimini IV wares, derived from type 3 alluvial clays form a narrow compositional group rich in calcium (>6%) and chromium (>250 ppm), indicating a high degree of standardization. Indeed, this ware is one of the earliest examples of considerable pottery specialization in the European Neolithic. In contrast to this, the Incised Classic Dimini ware spreads out widely in a Ca−Cr plot, indicating that pottery of this particular style was produced at many sites outside Dimini, and was exchanged and distributed widely. As suggested by Schneider *et al*. (1990), the ancient potters might have realised that a light-coloured ceramic body was more important as a background for a visually contrasting, red-painted decoration than for incised patterns. Hence, there was no need to standardize the calcium content of the clay destined to produce incised pottery.

In conclusion, from chemical analyses of the pottery and relating their results by multivariate clustering, a much more complex picture emerges than previously assumed by classic archaeologists. According to this new view, Neolithic pottery production in Thessaly was already surprisingly standardized, realised by selection of specific raw materials, an improved kiln technology that may have achieved temperatures as high as 1000ºC for the most advanced pottery, as well as abundance and diversity of decorating pigments and their application techniques. Hence, the transition from rather crude, low-fired Middle Neolithic Sesklo III pottery to Late Neolithic Tsangli-Larissa (Dimini I) fine decorated ware was accompanied by impressive and intensive technological and stylistic innovation (Schneider *et al*., 1991). Subsequently, during the Late Neolithic to Early Helladic periods Thessalian potters used calcareous clays to brighten the appearance of their pots. Calcareous clays provide both artistic and technological benefits. Aesthetically, on these light surfaces, several black and red pigments would create strikingly beautiful contrasting colourations (Fig. 12a). Technologically, the combination of calcareous ceramic bodies and illitic slips was very fortuitous as the engobe surface layers adhered well to the body owing to the small gradient in the coefficients of thermal expansion. In addition, lower firing temperatures were required to obtain dense ceramics owing to the fluxing properties of CaO.

4.1.4. Bronze Age Cretan (Minoan) pottery

Whereas Neolithic Aegean pottery was produced using free-forming techniques such as coiling, slab building and paddling, only in ~2000 BCE did Cretan potters regularly use a fast-spinning potter's wheel, at this time a radical advance in ceramic technology that enabled the artistic expression of clays in a much more sophisticated manner (Williams, 1997). The use of the potter's wheel is thought to have spread from Crete to mainland Greece around 1800 BCE, and from there to other parts of Europe.

Similar advances also pertain to the selection of raw materials. The examples of Early to Late Minoan pottery (Fig. 13) show clearly a development trend reflecting the desire of the ancient potters to boost the quality of their products by beneficiation of clay raw materials even though the still rather primitive kiln technology (Heimann and Maggetti, 2014) frequently counteracted their endeavours.

Chemical analyses reveal that the composition of Cretan pottery changed with time in response to technological developments and possibly aesthetic requirements. Figure 13a depicts the phase triangle $CaO-A1_2O_3-SiO_2$ with the binary compounds wollastonite ($CaSiO_3$, Wo) and mullite ($3A1_2O_3{\cdot}2SiO_2$, Mu), as well as the ternary compounds anorthite ($CaA1_2Si_2O_8$, An) and gehlenite ($Ca_2A1_2SiO_7$, Ge).

The open circles refer to Neolithic pottery made from low-calcareous clays found at Phaistos in southern Crete, the solid circles to pottery from very calcareous clays found at Knossos in northern Crete. The Phaistos samples are situated in a compositional triangle formed by the conodes quartz–anorthite, anorthite–mullite and mullite–quartz. Thus, the equilibrium composition should consist of the mineral assembly quartz + mullite + anorthite (glass) similar to that of stoneware or porcelain. However, low-firing temperatures, presumably close to or below 600ºC, prevented the attainment of this equilibrium composition. In addition, because small amounts of residual primary dolomite occur in the shards, and dolomite decomposes at 550ºC in oxidizing ceramic firing, its preservation in the ceramic body also points to very low firing temperatures. The Neolithic Knossos ceramic bodies are highly calcareous, and occupy

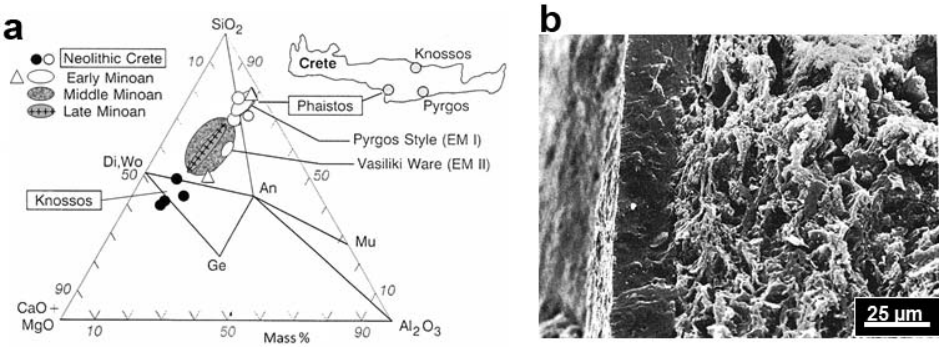

Figure 13. (a) Composition of Neolithic Crete and Bronze Age Minoan ceramics in the ternary phase diagram $CaO-Al_2O_3-SiO_2$ (Heimann, 1989; data after Noll, 1982). (b) Scanning electron microscopy image of the black, highly vitrified engobe (left) on a porous ceramic body of Middle Minoan Kamares ware (Noll, 1982; in Heimann and Maggetti 2014). With permission by Schweizerbart Science Publishers.

the compositional triangle anorthite–gehlenite–wollastonite. Low firing temperatures, however, prevented the formation of equilibrium high-temperature phases such as gehlenite and diopside. Large amounts of pristine calcite grains are still present in the shards. Here, the solidification has been attained solely by shrinkage due to thermally induced dehydration of the clay matrix and the concomitant increase of packing density of the clay particles, with only marginal mediating action of true sintering processes. In this context it should be noted that the apparent absence of gehlenite might be related to either thermal reactions beyond 950ºC, forming anorthite during unintentional kiln temperature excursions or chemical decomposition forming a sequence of zeolites or calcium carbonate during burial in soils saturated with carbon dioxide and/or humic acids (Heimann and Maggetti, 1981). Figure 14 shows an example of scalenohedral calcite crystallites formed within a pore space of a Late Minoan pottery shard and attributed to the decomposition during burial of initially formed gehlenite (Noll, 1982).

The characteristics of ceramics changed considerably during the Early Minoan (EM) period. Although Pyrgos-style ware of Late EM I (*ca*. 2600 BCE) still shows many features akin to those of the Neolithic Phaistos pottery the compositional field of which it partly shares (open ellipses), sintering of the clay matrix attests to an improvement of the technology through higher firing temperatures. The Vasiliki ware of EM II (*ca*. 2000 BCE) became more lime-rich with a comparatively narrow distribution of the alumina content. The presence of small amounts of the equilibrium phase diopside points to a firing temperature >850ºC. Early Minoan potters may have realised that it was more advantageous to use calcareous clays rather than non-calcareous ones as the former resulted in a denser fabric at moderate firing temperatures. On the other hand, highly calcareous clays, similar to those from which the Neolithic Knossos pottery was made, yielded pottery prone to lime spalling because of the presence of residual free CaO from the thermal decomposition of calcite. Only if the firing temperatures exceeded 850 to 900ºC and were maintained for sufficient time, could free CaO combine with alumina and silica released by the thermal decomposition of clay minerals to form high-temperature so-called 'index' minerals such as diopside, gehlenite and anorthite.

Middle Minoan (2160/1970–1600 BCE) potters improved both the quality of the raw clay materials and the firing technology. Their high-quality Kamares ware (mottled

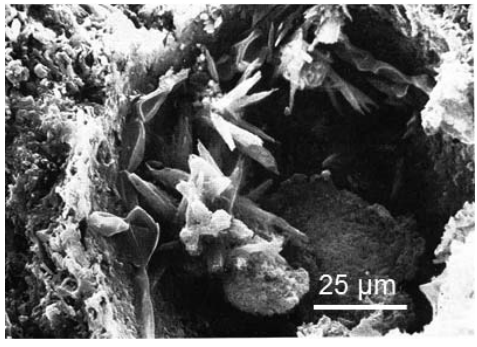

Figure 14. Calcite crystallites within a pore of a Late Minoan ceramic shard presumably formed by decomposition of gehlenite during burial (Noll, 1982). With permission by Schweizerbart Science Publishers.

grey ellipse in Fig. 13a) is now squarely located in the compositional triangle quartz–anorthite–wollastonite, the 'ceramic triangle'. Kamares pottery generally contains less alumina than Early Minoan ware. Diopside is now abundantly present, calcite is usually absent, but gehlenite is still only rarely visible in X-ray diffractograms. Hence, all these features point to a maximum firing temperature in the range 900 to 950ºC. Later Kamares ware may have been fired at still higher temperatures around 1050ºC, because in the white parts of the painted decoration proto-enstatite ($MgSiO_3$; Smith, 1959) formed by thermal decomposition of talc ($Mg_s[(OH)_2Si_4O_{10}]$), applied to the leather-hard body prior to firing (Noll, 1982) (Fig. 11b). Hence, the occurrence of proto-enstatite constitutes an important temperature marker for this particular type of pottery. The onset of formation of enstatite from talc in reducingly fired Mg-rich calcareous illitic clays has been determined to be ~850ºC (Görres *et al.*, 2000). Figure 13b shows in an oblique view the interface between densely sintered engobe and a porous ceramic body of Middle Minoan Kamares ware.

Finally, during the Late Minoan period (1600/1580–1070 BCE), the processing and firing technologies of the pottery were further improved. The variation ellipse (light grey with crosses in Fig. 13) has narrowed considerably pointing to a very effective compositional control of the alumina/silica ratio, presumably by standardizing the ratio of plastic clay to non-plastic inclusions. This even suggests that the Late Minoan potters had learned to blend clays from different sources with different lime contents and workability to achieve a consistent product. In addition, efficient elutriation of the raw clay materials presumably removed coarse constituents such as calcite grains. Ceramics lower in lime and richer in silica shown in the variation ellipse originate from Mochlos, Gournia and Pseira along the northern coast of Crete, whereas the samples richer in lime and lower in silica were found at Knossos, Haghia Triada (Belfiore *et al.*, 2007) and Phaistos. The estimated firing temperature was ~1050ºC (Heimann and Franklin, 1979) as judged by the high proportion of closed near spherical pores, and the highly sintered and slightly vitrified ceramic matrix.

4.2. Medium high-fired earthenware

The prototypical Roman medium high-fired earthenware is known as Terra Sigillata which was produced in virtually all parts of the Roman Empire, from Italy to Spain to Gaul to Britain to Syria. Owing to its ubiquity, it has been dubbed the Roman *'leitfossil'* (type fossil; Bemmann, 1993). Indeed, Roman pottery has been exported from Italy since the 4th century BCE, first as so-called Campanian Ware, a black-surfaced pottery type, followed in the mid-1st century BCE by Terra Sigillata, a red slipped ware produced initially in Arretium (modern Arezzo) (Fig. 15a). Terra Sigillata pottery workshops flourished between the 1st century BCE and about the 4th century CE. This mass-produced pottery was highly standardized and their forms and types (Dragendorff, 1895, 1896; Déchelette, 1904; Knorr, 1919) were limited to a few practical forms for easy stacking and transport. The ware was produced from calcareous illitic clays that were collected carefully, processed thoroughly by elutriation and settling and fired between 950 and 1050ºC in special kilns. In these kilns, the ware was prevented from reacting with hot-flame gases by

Figure 15. (a) Italian Terra Sigillata bowl (type Conspectus 34.1) from Arretium, Italy (30−100 CE). Workshop of C. Jul. Firmicus. Reg. No. 1814,0704.1558. AN 00894802. © The Trustees of the British Museum, London. (b)Terra Sigillata picture bowl (type Dragendorff 29) from La Graufesenque, Southern Gaul. (20-40 CE). Workshop of Bassus and Coelus. Height 10 cm, diameter 22.5 cm. Reg. No. 1869,0205.5. AN 00469677. © The Trustees of the British Museum, London.

channelling the latter through terracotta pipes away from the product. The finest clay fraction (<2 μm), obtained as the last fraction during settling with a large amount of illite, was used as a slip (engobe) into which the leather-hard vessels were dipped prior to firing. Roman potters also used slips with greater viscosity to trail on decorations by the so-called barbotine technique. Plain undecorated pottery vessels for domestic consumption were formed on a potter's wheel. In contrast to this, the production of the celebrated picture bowls catering to the refined taste of the affluent portion of Roman society involved pressing or throwing wet clay into an unglazed ceramic mould adorned with impression of stamps or '*sigilla*' from which the ware obtained its descriptive name (Fig. 15b).

During oxidizing firing, the potassium- and iron-rich illitic slip transformed into a partially vitrified, highly glossy and bright red, hematite-containing surface coating. Firing under reducing conditions and subsequent 'smoking' of burnished ware produced shiny black surfaces by incorporation of elemental carbon (soot). This type of pottery is known as 'Terra Nigra'. However, true black Terra Sigillata was produced from calcareous clay coated with a slip made from non-calcareous iron-rich illitic clay that after reducing firing turned black owing to the formation of magnetite below 950ºC and an additional hercynite phase at firing temperatures exceeding 950ºC (Maggetti and Galetti, 1986; Fig. 6a). A subsequent oxidizing firing step turned the porous ceramic body red again due to formation of hematite whereas the dense surface layer maintained its glossy black appearance. This was precisely the technology applied by Attic potters to make their celebrated black-on-red ware.

Figure 16 shows that the ceramic bodies of Terra Sigillata vary within narrow compositional bounds whereby the ware from Italian Arezzo is slightly more siliceous and less aluminous than that of the southern Gaulish workshops of La Graufesenque.

Much effort has been expended on the determination of the provenance, assignment of workshops, trade pattern and production techniques of Roman pottery. This endeavour has been aided by the use of ceramic reference groups (Schneider and

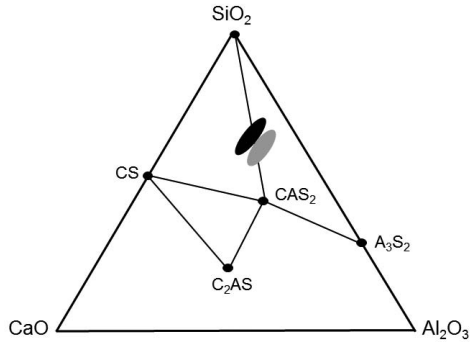

Figure 16. Compositional scatter of Terra Sigillata bodies from Arezzo, Etruria, Italy (black area, 256 analyses) and La Graufesenque, southern Gaul, France (grey area, 139 analyses). Symbols are as in Fig. 20.

Hoffmann, 1990) that are characterized by a unique combination of elements and their concentrations, thus providing a geochemical fingerprint to distinguish among workshops and provenance. For example, Fig. 17 shows the fit of Terra Sigillata, definitely produced by the Roman potter Lucius Gellius, with the reference groups 'Arretium' (Arezzo) and 'Lugdunum' (Lyon) in a bivariate TiO_2/MgO plot. Apparently, the potter worked in both places even though the spread of the compositional pattern suggest that pottery produced by Gellius (open circles) may have been altered by selective dissolution of alkali and alkaline earth elements during burial thus increasing the relative concentration of more environmentally stable elements such as titanium, aluminium and iron. On the one hand, samples with greater TiO_2, and generally also elevated phosphorus levels, may actually belong to the bulk of the Arezzo and Lyon populations. On the other hand, the high Mg concentration combined with lower TiO_2 levels cannot be explained easily by alteration during burial.

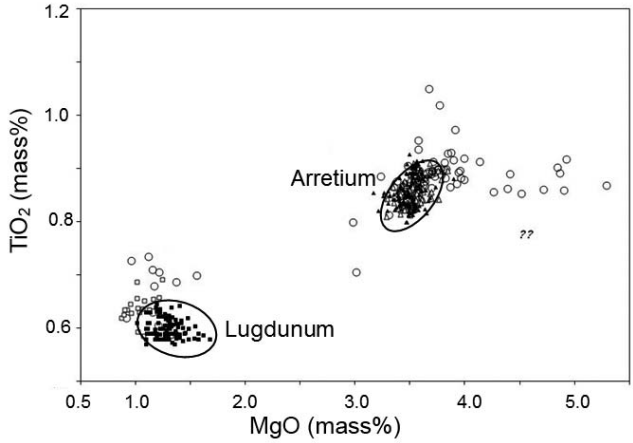

Figure 17. Bivariate plot of the titania and magnesia concentrations of Terra Sigillata produced by the potter Lucius Gellius (open circles) and of the ceramic reference groups for Terra Sigillata from Arretium (Arezzo) and Lugdunum (Lyon) (variation ellipses). From Schneider and Daszkiewicz (2006), where the exact meaning of "*??*" is also explained.

Instead, this feature may indicate the existence of a different workshop or production centre within the Lyon and Arezzo regions (Schneider and Daszkiewicz, 2006).

As mentioned above, almost all Roman Terra Sigillata has been manufactured from calcareous illitic clays. Indeed, such clays were used nearly exclusively for Italian Terra Sigillata from Arezzo and Padana, and provincial ware from southern (La Graufesenque, Banassac, Montans), central (Lezoux, Lyon) and eastern (Blickweiler, Chèmery-Faulquemont, Rheinzabern, Trier) Gaul (Picon *et al*., 1971). The use of calcareous clays has several technological advantages (Tite *et al*., 1982). First, a calcareous clay body has a significantly higher thermal expansion coefficient of $(4.5-7.0)\times10^{-6}$ ºC^{-1} than that of comparable non-calcareous clay bodies with $(2-3.5)\times10^{-6}$ ºC^{-1}. Hence, its thermal expansion coefficient will match more closely that of the partially vitrified slip that has a thermal expansion coefficient in the range of $(5-10)\times10^{-6}$ ºC^{-1}. Consequently, there will be a smaller risk of slip-crazing or even delamination during cooling. Second, calcareous clays produce bodies with greater rigidity and compressive strength owing to the ready formation of crystalline mineral phases (Peters and Iberg, 1978). The resulting pottery is, therefore, tougher and more resilient when used as domestic tableware and, in particular, for use by the Roman military. The inevitable breakage of earthenware encountered during transport over long distances on rocky roads required continuous replacement. Hence, each legion had an associated contingent of potters.

The sintering and, eventually, vitrification processes of the calcareous illitic clays used by Roman potters in their Terra Sigillata workshops can be described quantitatively by defining two stages during which the microstructural changes are brought about by different mechanisms. Stage 1 between ambient temperature and 900ºC is governed by solid-state dehydroxylation of clay minerals, leading to a close-to-linear mass loss that causes shrinkage-related changes of the fabric imposed by the formation process of the ceramic body. In stage 2 beyond 900ºC, the reactions associated with mass loss have ceased to occur, and microstructural changes occur by changes in the pore volume that is, sintering *sensu strictu* caused by sealing of open pores. The densification obtained during these two stages can be expressed by the volume quotients V_{900}/V_0 and V_T/V_{900} as

$$\frac{V_{900}}{V_0} = \left(1 - \frac{\Delta m}{m}\right) \frac{\rho_{900} - R_{900}}{\rho_0 - R_0} \cdot \frac{\rho_0 R_0}{\rho_{900} R_{900}} \tag{5}$$

$$\frac{V_T}{V_{900}} = \frac{\rho_T - R_T}{\rho_{900} - R_{900}} \cdot \frac{\rho_{900} R_{900}}{\rho_T R_T} \tag{6}$$

whereby m is mass of clay, Δm is the mass loss between ambient temperature and 900ºC, V_0 pore volume of the dried ceramic body. Furthermore, V_{900} and V_T are the pore volumes at 900ºC and $T > 900$ºC, respectively; ρ_0 is the specific gravity of the dried ceramic body, ρ_{900} and ρ_T are the specific gravities at 900ºC and $T > 900$ºC, respectively; R_o is the volumetric density of the dried ceramic body, and R_{900} and R_T are the volumetric densities at 900ºC and $T > 900$ºC. Plotting V_T/V_{900} against firing

temperature yields an S-shaped curve (Fig. 18) whereby $V_T/V_{900} = 0.8$ is defined as the temperature of the onset of densification and $V_T/V_{900} = 0.5$ to the mid-point sintering temperature (Heimann, 1978/79).

The steep negative slope of the sintering curve of a calcareous clay suggests an extremely narrow firing interval of only 15–25ºC as suggested by the small difference between the onset of densification (V_T/V_{900} = 0.8 at 1015ºC) and the mid-point of sintering ($V_T/V_{900} = 0.5$ at 1035ºC). Hence, such clays require very strict control of the firing temperature in order to avoid undesirable slumping and warping of the ware caused by rapid formation of grain boundary melts with subsequent destabilization of the vessel. The rise of the sintering curve beyond 1150ºC can be explained by bloating, that is, swelling caused by the expansion and subsequent expulsion of air trapped in closed pores (Maniatis and Tite, 1975).

After a period of considerable economic success, the factories at Italian Arretium began to decline both in their technological and aesthetic aspects in the 1st century CE and hence, gave way to the ascent of factories in the Roman province of Gaul. However, the economic importance of the latter also decreased at the end of the 2nd century CE and their place, in turn, was taken by pottery factories in Roman North Africa, principally in the areas of modern Tunisia and Libya (Leptis Magna).

To demonstrate essential technological aspects of Gaulish Terra Sigillata wares, a comparison is shown (Fig. 19) of the densification of the ceramic body of eastern Gaulish Terra Sigillata from Tabernae (today's Rheinzabern) with those of other provincial Roman potteries from southern (La Graufesenque, G) and eastern Gaul (Chémery-Faulquemont, C and Blickweiler, B). The lower $SiO_2/(Al_2O_3+K_2O)$ (quartz/illite+chlorite) ratios, in particular larger amounts of fluxing K_2O, of both La Graufesenque and Blickweiler Terra Sigillata, lead to greater densification compared to wares and moulds from Rheinzabern as well as Chémery-Faulquemont. The fact that densification of Blickweiler ware exceeds that of ware from La Graufesenque despite

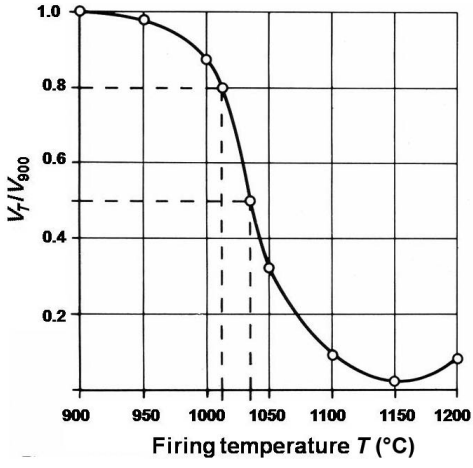

Figure 18. Typical sintering curve of calcareous illitic clay fired in air (Heimann, 1978/79). V_{900} and V_T are the pore volumes at 900ºC and at $T > 900$ºC, respectively.

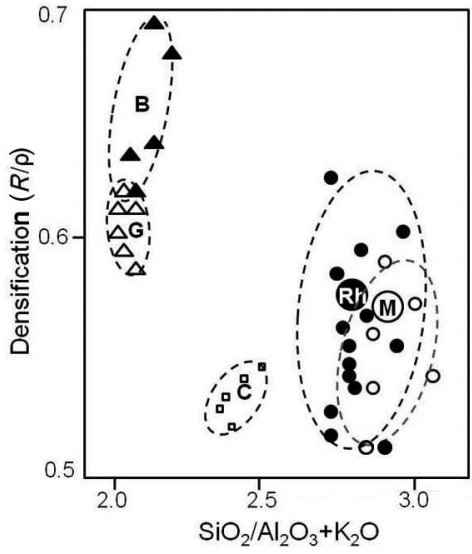

Figure 19. Density coefficient (densification) R/ρ of eastern (Rheinzabern Rh, M; Chémery-Faulquemont, C; Blickweiler, B) and southern (La Graufesenque, G) Gaulish Terra Sigillata as a function of the quartz/clay ratio, expressed as the ratio $SiO_2/(Al_2O_3+K_2O)$. *R* refers to raw density, *i.e.* density with pores; ρ refers to specific gravity, *i.e.* density without pores. The large circles Rh and M denote the averages of Rheinzabern ware and moulds, respectively (Heimann, 1982).

almost identical quartz/clay ratios suggests somewhat higher firing temperatures of the former, which were due to improved kiln technology.

4.3. High-fired stoneware and porcelain

Firing of non-calcareous illitic and kaolinitic clays at temperatures >1200ºC has been achieved over time in ever more sophisticated ceramic kilns and has resulted in stoneware pottery with increased mechanical and chemical stability, much reduced porosity, and smooth shiny surfaces owing to the presence of wood ash-derived and, later, salt and feldspathic glazes.

Stoneware can be considered the historical precursor of true hard-paste porcelain from which it is distinguished by its generally coloured nature, its lack of translucency and some remaining porosity. It had already been produced in copious amounts in China during the late Shang dynasty (~1700–1028 BCE) and reached its acme during the Han (202 BCE–220 CE) and Yuan (1279–1368 CE) dynasties. Many of the early stoneware products were coated with a greenish celadon glaze thought to imitate highly priced jade. Important stoneware traditions existed in Japan, Korea and the Indochinese realm including Thailand, Laos and Vietnam. At the beginning of the 14th century CE, a special development occurred in the Rhenish part of Germany (Frechen, Cologne and Siegburg) based on high-refractory clays that reached its zenith between about 1440 and 1620 CE. The products were blue-greyish plates, bowls and drinking vessels, salt-glazed to improve their appeal and to provide added smoothness to aid easy cleaning.

4.3.1. Chinese stoneware (proto-porcelain)

The clay raw materials landscape of China is characterized by two main types of clay that are separated by a distinct geographical dividing line, the Nanshan–Qinling (N–Q)

divide or kaolinite-porcelain stone (*petuntse*) line, also known as clay-rich/quartz-rich division line. The clays used for high-temperature ceramics located north of this line are rich in true clay minerals derived from sedimentary strata. These highly refractory clays contain ~40 mass% alumina, mostly fixed in kaolinitic clay minerals. By contrast, micaceous clays found south of the divide have formed mostly from weathered feldspar of igneous, predominantly granitic, rocks and contain comparatively small amounts of clay minerals but large amounts of fine quartz and secondary potassium mica (sericite) instead. Consequently, their alumina content is <20 mass%. White-firing, *i.e.* iron-poor versions of these rocks are referred to as 'porcelain or china stone' (*petuntse*) and constitute the mainstay of 'true' Chinese porcelain produced at the important kiln site of Jingdezhen, Jiangxi province from the 10th century CE onwards and reaching its perfection during the Song, Ming and Qing dynasties.

Typical proto-porcelain, *i.e.* high-fired stoneware (Yin *et al.*, 2011) shows a composition of the ceramic body of 75–80 mass% SiO_2, 15–18 mass% Al_2O_3, ~2 mass% K_2O, ~2 mass% Fe_2O_3, and 1–1.5 mass% each of CaO, Na_2O, MgO and TiO_2. This composition is essentially that of true porcelain, and is consistent with the mineralogy of the clays occurring south of the N–Q divide which are dominated by micaceous porcelain stone (*petuntse*). The shiny greenish glaze of the proto-porcelain greenware is composed of 60–70 mass% SiO_2, ~15 mass% Al_2O_3, 10–20 mass% CaO, <3 mass% MgO, 2–3 mass% K_2O and 2–4 mass% Fe_2O_3. The glazing process was based primarily on eutectic-melt formation during firing, during which lime-rich material reacted with the surface of the ceramic body to form a vitreous glaze with a composition determined by the firing temperature, and possibly the duration of firing (Yin *et al.*, 2011). The source of the lime-rich glazing material was washed wood ash, high in CaO and low in K_2O. The difference in composition between the ceramic body (B) and the applied glaze (G) is shown in Fig. 20.

The exact compositions of the glazes were automatically tuned by a temperature-controlled mechanism through selective absorption of ceramic material into the melting glaze. The lime-rich compound interacted with the material of the ceramic body to form a calcium aluminium silicate glaze at an assumed firing temperature of 1200–1250ºC. Figure 21a shows a glazed stoneware dish produced during the Yuan dynasty at the Imperial Jiaotanxia Guan kiln at Hangzhou, Zhejiang province.

4.3.2. Chinese porcelain

Arguably, true high-fired porcelain ware with a white translucent body originated during the Sui (581–617 CE) and Tang (618–906 CE) periods even though some scholars maintain that it was already produced in Zhejiang province during the Eastern Han (25–220 CE) period. During the Song (960–1279 CE) and Mongol Yuan (1279–1368 CE) dynasties, Chinese ceramic workmanship reached one of its most brilliant phases with the famous monochrome Longquan celadon porcelaneous stoneware. However, it was not until the late 14th century CE that the techniques of painting porcelain in polychrome underglaze and overglaze colours were developed and brought to technical perfection during the Ming (1368–1644 CE) and Qing (1644–1912 CE) dynasties.

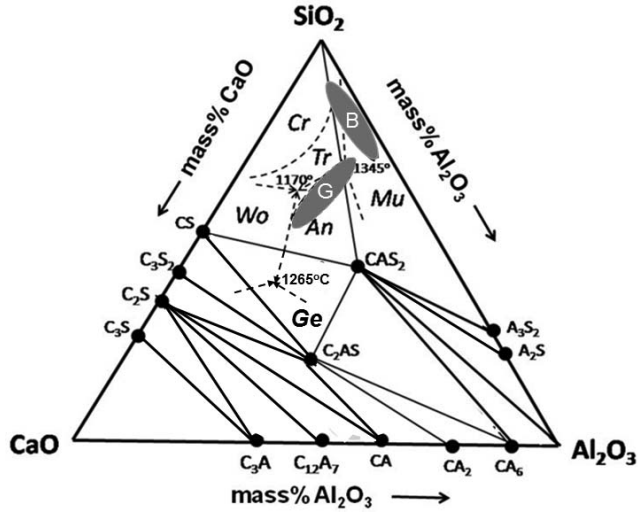

Figure 20. Compositional scatter ellipses of the body (B) and the glaze (G) of Chinese proto-porcelain from the Deqing site of Zhejiang province (Yin *et al*., 2011), located in the 'ceramic triangle' $CaO-Al_2O_3-SiO_2$. Three important triple points are indicated at the intersection of the phase boundaries (dashed lines). An – anorthite, CAS_2; Cr – cristobalite, SiO_2; Ge – gehlenite, C_2AS; Mu – mullite, A_3S_2 to A_2S; Tr – tridymite, SiO_2; Wo – wollastonite, CS. CS is the composition of wollastonite in cement chemical notation, meaning $CaOSiO_2$. The binary and ternary phases are denoted according to the cement chemical notation, C = CaO, $A = Al_2O_3$, $S = SiO_2$.

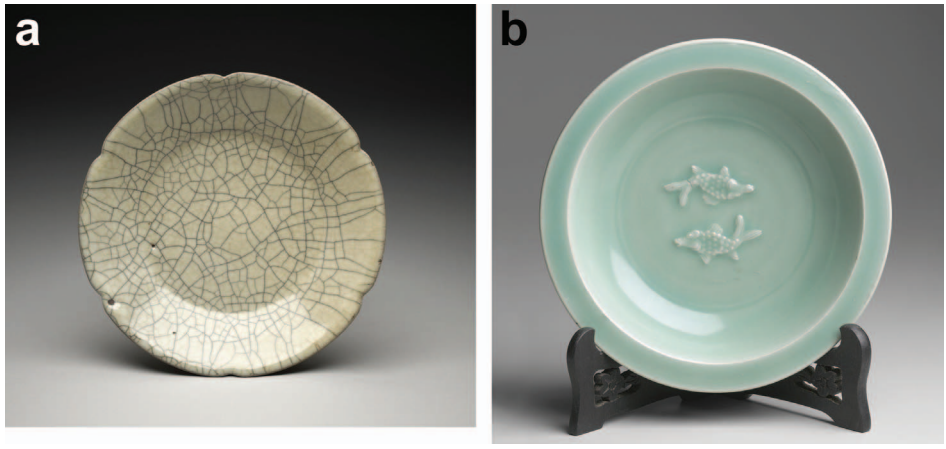

Figure 21. (a) Guan stoneware dish with craquelling celadon glaze. Yuan dynasty (1279–1368). Hangzhou, Zhejiang province. Height 3 cm, diameter 16.4 cm. Reg. No. PDF.69. AN 1051096. © The Trustees of the British Museum. London. (b) Longquan celadon-glazed porcelaneous dish with twin fish decoration. Southern Song dynasty (12^{th} to 13^{th} centuries CE). Diameter 22 cm. Reg. No. 43.1. © Minneapolis Institute of Arts, The John R. Van Derlip Fund.

By its nature, ancient Chinese porcelain was soft-paste porcelain, produced from kaolinite (china clay), *petuntse* or china stone ('pottery stone'), the historic term for a wide range of micaceous or feldspathic rocks, and fine quartz sand. It was fortuitous that Nature provided a ready-to-use mix of these minerals at Jingdezhen, Jiangxi Province in southern China. This enabled Chinese potters to process the natural raw materials at temperatures between 1250 and 1300ºC, without any modification other than cleaning and aging of the clay mix. As a result, Jingdezhen became the main production hub for Imperial porcelain during the Southern Song dynasty (1127–1279 CE). Porcelain produced at Jingdezhen was highly cherished as it was said to be as white as jade, as bright as a mirror, and as thin as paper (Schroeder and Erickson, 2014).

Today, Chinese scholars use the term 'porcelain' in a broad sense that includes fine, hard dusky and grey micaceous mineral-based materials fired to a vitrified state such that they emit a musical note when struck. In contrast to this, their Western colleagues prefer the term 'porcelain' in a narrower sense for fine, hard, white and translucent pottery. They also distinguish between hard-paste (*pâte dure*) calcareous (early Meissen, Vienna, some Sèvres) and feldspathic (also called triaxial) porcelains, produced from kaolin (china clay), micaceous feldspar (also called *petuntse*, china stone, porcelain stone) and quartz, and soft-paste (*pâte tendre*) porcelain, made from ground fused glass and mixed with clay or some other ingredients (Section 4.3.5.). Whereas most Far Eastern porcelains were fired only once below 1320ºC with a likely average of 1280ºC, Western hard-paste porcelains such as Meissen ware (Section 4.3.4.) were treated to higher temperatures, often in excess of 1400ºC, fired twice (biscuit and glaze firing), and covered with a clear, transparent feldspathic glaze. Application of overglaze colours would require a third firing.

The ceramic body of Longquan porcelaneous celadon ware consists of a mixture of finely ground *petuntse* (china stone), kaolinitic clay and some red-firing clay that would contrast admirably with the blue-green jade-like glaze (Wood and Rastelli, 2014). Firing to temperatures of 1240–1260ºC causes the clay to break down completely and transform to clusters of small 2:1 mullite needles and some silica glass. The feldspar component of the china stone will be converted to larger prismatic 3:2 mullite crystals and more glass into which quartz crystals dissolve (Fig. 22a). This means that there are two generations of mullite with different origins, compositions and physical appearance (Tite *et al*., 2012; see also Section 4.3.3.). On cooling, residual quartz grains undergo a displacive phase transformation at 573ºC from high quartz to low quartz, accompanied by shrinking, causing the glass adhering to the quartz grains to crack. As more and more quartz dissolves in the silicate glass during prolonged firing, the viscosity of the glass increases and provides strength to the ceramic body, that is, resistance to slumping. The mullite needles, acting as efficient reinforcement, augment this structural strengthening.

The longstanding enigma that is the translucent, soft and in its ethereal beauty unique lustre of the glaze of Longquan celadon ware (Fig. 21b) was solved eventually through the work of Kingery and Vandiver (1986). Figure 22b shows schematically a cross-

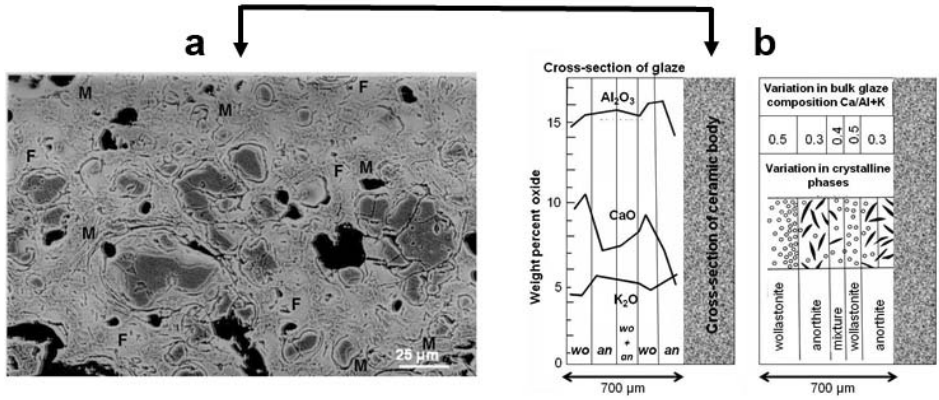

Figure 22. (a) Backscattered electron image of Longquan celadon ware body, etched for 3 min in 2% hydrofluoric acid. Quartz grains appear as dark grey, surrounded by rims of glass and cracks related to the displacive high–low phase transformation of quartz. There are clusters of filaments consisting of secondary mullite (M) as well as glassy pools containing elongated mullite crystals (F) in a continuous matrix (Tite *et al.*, 2012). Image courtesy of Prof. Michael Tite, Oxford, UK. (b) Variation in composition across the glaze of a Longquan celadon shard, showing a structure consisting of alternate zones comprising wollastonite and anorthite crystallites. Modified and redrawn after Kingery and Vandiver (1986).

sectional view of the glaze, characterized by local variation in composition on a scale of <100 µm. The left panel of Fig. 22b depicts the uneven distribution of Al_2O_3, CaO, and K_2O across the glaze that leads to precipitation of nano- to micro-sized needle-shaped crystallites of anorthite in places where the alumina content is high and the lime content is low. Likewise, wollastonite crystallites precipitate in regions high in CaO and low in alumina. The resulting zoning shown in Fig. 22b is at the heart of the optical performance of the glaze. Both wollastonite and anorthite can form from the viscous calcium aluminium silicate glass if mixing is restricted by high viscosity and the bulk glass composition is similar to that of the crystalline precipitates. Hence, in the $CaO-Al_2O_3-SiO_2$ phase diagram shown in Figs 3 and 20, the composition of the crystallites varies along the Wo–An join.

Longquan celadon ware was fired in hill-climbing (dragon) kilns of considerable lengths, up to 70 m or more. In the largest of these kilns, up to 100,000 ceramic pieces could be fired in a single firing cycle at temperatures as high as 1240–1260ºC (N. Wood, pers. comm. 2012). During the Yuan dynasty, further advances in firing technology allowed very large dishes and jars to be made for export purposes in great quantities. However, their quality, and in particular the optical properties of their glazes, never reached those of the Song wares.

4.3.3. Thai stoneware

As early as the 10th century CE, potters living in what today is Thailand developed independently a ceramic tradition that was increasingly influenced by the technology of their northern neighbours in China, but without achieving the technological competency of their Chinese potter colleagues. Nevertheless, the wealth and prosperity

of the state of Sukhothai (1238– ~1438 CE) depended to a large extent on the manufacture and export of high-quality stoneware that was hugely popular and widely traded throughout the southeast Asian realm. During the Sukhothai reign, glazed stoneware known as '*sangkhalok*' was produced in large quantities at the kilns of Sukhothai and Si Satchanalai but also at other kiln sites in northern Thailand including Kalong, Phan, Phayao and San Kamphaeng (Shaw, 2008, 2009).

The clays used by the potters of northern Thailand were kaolinitic, and the mineralogical phase composition of the stoneware body consisted of 9–14 mass% mullite, 15–26 mass% quartz and a balance of a glassy phase (Kilb, 1979; Heimann, 1989). This composition is located in the compositional triangle mullite—K-feldspar–quartz of the ternary system K_2O–Al_2O_3–SiO_2 (Fig. 23a). The relatively high proportion of fluxing K_2O leads to partial melting during firing at 1200ºC or beyond. The ternary eutectic point is at ~10 mass% K_2O, 11 mass% Al_2O_3 and 79 mass% SiO_2, at the junction of the stability fields of mullite, K-feldspar and quartz. The associated ternary eutectic temperature is 985ºC, *i.e.* firing of the clay at this temperature produces partial grain-boundary melts of the composition of the ternary eutectic. Indeed, the chemical composition of the Si Satchanalai ware shown in Fig. 23a is close to that of the ternary eutectic composition.

At this point, it is necessary to describe the thermal reactions of kaolinite in more detail. Firing of a kaolinitic clay leads to a structural collapse between 500 and 600ºC with the formation of a more or less amorphous dehydroxylated 'metakaolinite' phase. This phase transforms at >900ºC to an Al–Si spinel (AS_2, $Al_2O_3 \cdot 2SiO_2$). This spinel, in turn, releases silica as cristobalite when heated beyond 1100ºC to form Al-rich primary platy mullite (2:1 mullite, $2Al_2O_3 \cdot SiO_2$). At even higher temperatures, the amount of melt present in the ceramic body increases, and eventually Si-rich secondary needle-

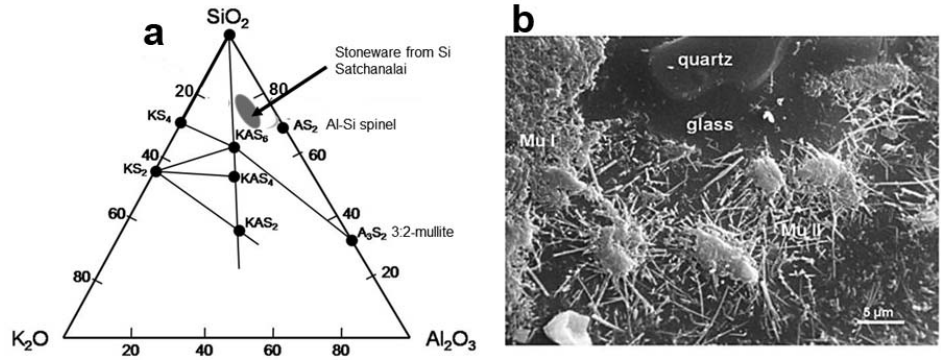

Figure 23. (a) Compositional scatter ellipse of stoneware from Si Satchanalai, Thailand, in the ternary phase diagram K_2O–Al_2O_3–SiO_2 (Heimann and Maggetti, 2014). (b) Scanning electron microscopy image of the ceramic body of stoneware from Si Satchanalai showing primary platy mullite (Mu I, left) and secondary needle mullite (Mu II, centre) as well as a quartz grain dissolving in glass (top) (Kilb, 1979). The firing temperature of the stoneware was estimated to have been between 1200 and 1250ºC (Kilb, 1979; Heimann, 1989). Image courtesy Dr. Lothar Kilb.

like mullite (3:2 mullite, $3Al_2O_3{\cdot}2SiO_2$) crystallizes directly from the melt (Schüller, 1964; Iqbal and Lee, 2000). Frequently, primary mullite provides a growth site for this crystallization process because of structural similarity between these two phases that form a solid solution series as shown in the binary $SiO_2-Al_2O_3$ phase diagram of Fig. 3a. The two limiting compositions of the mullite solid solution, *i.e*. platy mullite (Mu I) and needle mullite (Mu II) are shown in the SEM micrograph of the ceramic body of stoneware from Si Satchanalai, together with a quartz grain dissolving in glass (Fig. 23b). These two types of mullite can be distinguished from each other by careful XRD analysis supported by Rietveld refinement (Heimann, 2016).

4.3.4. Hard-paste porcelain of Meissen

The fascinating history of the discovery and technological development of European hard-paste porcelain of Meissen type has been described, for example, by Walcha (1981) and Heimann and Maggetti (2014). This unique ceramic ware is special as it is fired at such high temperatures that the mineral reactions both at grain boundaries and in the bulk are being controlled by nearly true thermodynamic relationships. Compared to East Asian porcelain, Meissen hard-paste porcelain had an entirely different development as it contains much less free quartz but more mullite. It also shows a substantially denser microstructure compared to Chinese and Japanese porcelains, related to its higher firing temperature that enabled quartz to be dissolved efficiently in the glassy phase. These facts induce drastically increased nucleation and growth of mullite crystals, and promote enhanced sealing of pores to yield a denser microstructure. In contrast to Chinese porcelain that is fired in a once-through cycle, Meissen porcelain is normally fired twice. The first (biscuit) firing occurs between 900 and 950ºC. After cooling, the white biscuit porcelain can be decorated by painting (underglaze decoration). After dipping in the glaze slurry and appropriate drying, the second firing (glost or glaze firing) is performed between 1200 and ~1500ºC. After cooling, the ceramic can be painted with enamel colours including gold and fired a third time at 700 to 850ºC to fix the enamel to the transparent glaze (overglaze decoration) Fig. 24a).

As shown in Fig. 25a, the chemical composition of the typical raw materials mix of 'triaxial' porcelain (50% kaolinite, 25% quartz, 25% (K-) feldspar) is located in the phase field of mullite at point 'A' (69.3 mass% SiO_2, 26.2 mass% Al_2O_3, 4.5 mass% K_2O). As the liquidus temperature (melting point) of this composition is beyond 1700ºC it will never be reached during ceramic firing as the typical firing temperature of contemporary Meissen porcelain is between 1370 and 1470ºC. Firing at and cooling from this temperature causes crystallization of mullite along the crystallization path A–B (dashed line) formed by connecting the point corresponding to the mullite composition through point 'A'. This crystallization path meets the phase boundary mullite–tridymite at 1280ºC at point 'B'. Further crystallization occurs when the system follows the phase boundary along the path B–C, until at 985ºC the ternary eutectic K-feldspar–tridymite–mullite is reached, at which point any liquid phase ceases to exist.

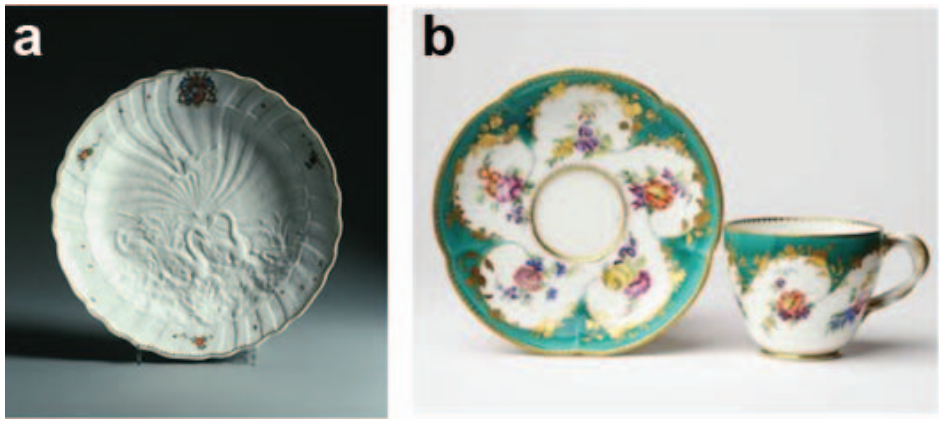

Figure 24. (a) Large bowl of the Swan service with overglaze decoration; Meissen (1737–1742). Diameter 43 cm. Inv. No. PE1427. © Staatliche Kunstsammlungen Dresden. (b) Soft-paste porcelain saucer and cup, painted with overglaze colours. Sèvres (1751–1757). Reg. No. C.1418A-1919 and C.1418-1919. © Victoria and Albert Museum, London.

Crystallization during cooling of the near-eutectic melt from high temperature leads first to formation of mullite, reaching a maximum amount of 27.4 mass% at 1280ºC.

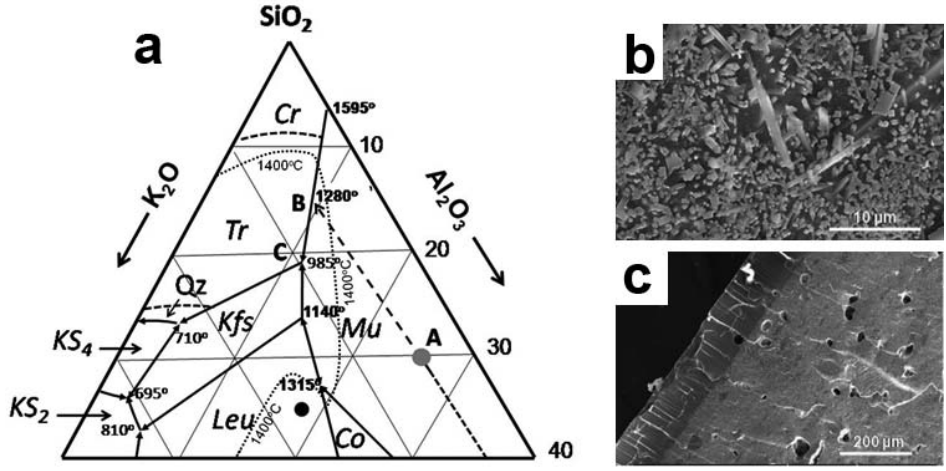

Figure 25. (a) Phase boundaries and coexisting phases in the SiO_2-rich section of the ternary system K_2O–Al_2O_3–SiO_2 (after Schairer and Bowen, 1947). The path A–B–C (dashed line) characterizes the crystallization history of a typical Meissen porcelain body. Co – corundum, Cr – cristobalite, Kfs – potassium feldspar, KS_2 – potassium disilicate, KS_4 – potassium tetrasilicate, Leu – leucite, Mu – mullite, Qz – quartz, Tr – tridymite. The ternary eutectic is at the triple point Kfs–Mu–Tr with the melting temperature of 985ºC. The dotted line shows the isotherm at 1400ºC. (b, c) Microstructure of historical Meissen porcelain from 1774. Mullite crystals in a glassy matrix (b) and contact zone between glaze and the ceramic body below (c). Images courtesy of Dr Bernd Ullrich, TU Bergakademie Freiberg, Germany.

Below this temperature, tridymite crystallization starts, reaching 22.9 mass% at 985ºC besides 47.4 mass% melt phase, and an additional amount of 2.3 mass% mullite. During further cooling to ambient temperature, crystallization of the remaining melt yields 26.6 mass% K-feldspar and an additional amount of 20.8 mass% tridymite. Hence, the thermodynamic equilibrium composition of the final porcelain body ought to be 29.7 (27.4 + 2.3) mass% mullite + 43.7 (22.9 + 20.8) mass% tridymite + 26.6 mass% K-feldspar (Salmang *et al*., 2007). In practice, however, the microstructure of a typical porcelain body is very different. It consists of ~30 mass% mullite and 70 mass% $K_2O-Al_2O_3-SiO_2$ glass (Fig. 25b,c) because the highly viscous melt thus formed freezes without crystallization. This is precisely the composition found in historical (see for example Ullrich and Ballmair, 2002; Ullrich *et al.*, 2010) and contemporary Meissen porcelains.

Figure 26 shows the reaction scheme leading to the microstructure of porcelain (see also Iqbal and Lee, 1999, 2000; Lee and Iqbal, 2001).

4.3.5. Soft-paste porcelain

The earliest attempts by European potters to replicate Chinese porcelains date back to the 16th century CE when soft-paste (frit) porcelain bodies, so-called Medici

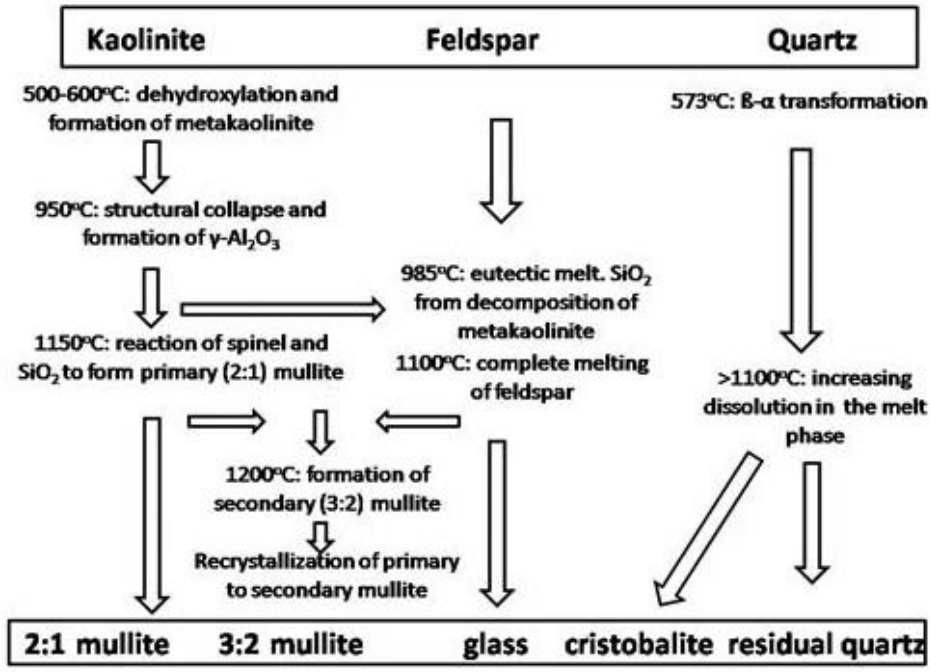

Figure 26. Simplified reaction scheme of formation of the microstructure of triaxial porcelain (adapted from Schüller, 1982; in Heimann and Maggetti (2014).

'porcelain', were crafted in Florence under the patronage of Grand Duke Francesco I de Medici. Medici 'porcelain' was manufactured by mixing a vitreous alkali silicate frit with white clay, feldspar and quartz. This 'surrogate' porcelain was re-invented some hundred years later in France and England, using traditional Near Eastern quartz-glass (frit)-clay compositions to copy East Asian porcelain. In France, this soft-paste (frit) porcelain is called *pâte tendre*.

In contrast to hard-paste porcelain, firing of soft-paste porcelain proceeds at considerably lower temperatures (biscuit firing at ~1100ºC, glaze firing at ~1000ºC). However, the decisive difference between hard- and soft-paste porcelain is not the firing temperature but the different sintering behaviour. The feldspar compound in hard-paste porcelain forms, with alumina and silica released from the kaolinite, a eutectic melt that is quenched during cooling and thus remains in the vitreous state without crystallizing (Zanelli *et al*., 2011). Hence, hard-paste porcelain contains up to 70 mass% of glass as opposed to the more crystalline microstructure of soft-paste porcelain, with only ~30 mass% of glass. This renders the latter more prone to mechanical destruction because it possesses lower hardness, abrasion resistance, bending strength and thermal shock resistance.

French soft-paste porcelains resemble Chinese porcelains in terms of translucency and whiteness. These soft-paste porcelains were produced in the 18th century CE in French manufactures at Saint-Cloud, Chantilly and Vincennes/Sèvres (fig. 24b). The frit used at the Vincennes/Sèvres pottery was a complex mix of sand, soda, calcined alum, calcined gypsum, saltpetre and rock salt, fired at the hottest part of the kilns to obtain a glassy substance. Subsequently, this frit was crushed, milled with chalk and marl, and finally shaped, mostly by moulding. The green ware was biscuit-fired at ~1100ºC for 4 days, then glazed and fired at ~1000ºC for use another day. The bodies of Sèvres porcelain consist of relict quartz and newly formed crystalline phases such as tridymite and wollastonite, all embedded in a glassy phase.

The simple ternary phase diagram Na_2O-SiO_2-CaO (Fig. 27a) is well suited to study equilibrium phase relationships of French soft-paste porcelain. The chemical analyses of porcelain bodies plot in the compatibility triangle connecting the phases [β-CS; β-wollastonite]–[NC_3S_6; devitrite]–[SiO_2; tridymite/cristobalite]. This is the equilibrium phase association for French soft-paste porcelains. It should be remembered that the simple three-component system shown in Fig. 27 does not consider K_2O and several other oxides that have a small but measurable impact on phase relationships, as well as on invariant and divariant equilibria. However, the simplified system can be used as a reasonably good approximation to reality. The region of interest shows two invariant points: (1) a ternary peritectic point at a temperature of 1035ºC with the four equilibrium (coexisting) phases [liquid L]–[β–CS]–[NC_3S_6]–[SiO_2] and (2) a ternary eutectic point at a temperature of 725ºC with the four equilibrium phases [liquid L]–[NS_2]–[NC_3S_6]–[SiO_2].

The 1100ºC isothermal section of this phase diagram illustrates the equilibrium composition attained during firing of French soft-paste porcelain bodies for five days at this temperature (Fig. 27b). According to theory, the phase assembly would be

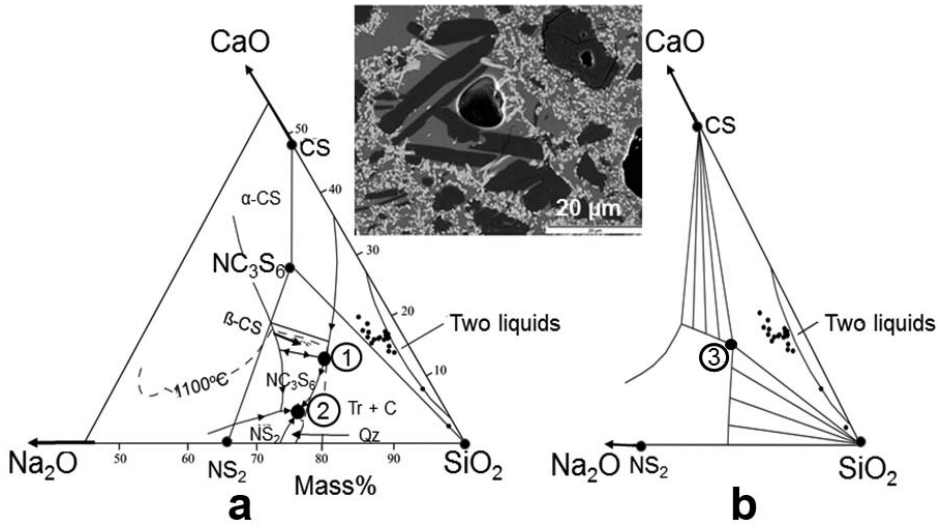

Figure 27. (a) Phase boundaries and coexisting phases in the high SiO_2 corner of the ternary system Na_2O–SiO_2–CaO (redrawn after Morey and Bowen, 1925). C – cristobalite, SiO_2; CS – wollastonite, $CaO{\cdot}SiO_2$; NS_2 – water glass, sodium disilicate, $Na_2O{\cdot}2SiO_2$; NC_3S_6 – devitrite, $Na_2O{\cdot}3CaO{\cdot}6SiO_2$; Qz – quartz, SiO_2; Tr – tridymite, SiO_2. **1** ternary peritectic point (1035ºC), **2** ternary eutectic point (725ºC). Dots = 17 analyses of French soft-paste porcelain (Brongniart, 1844, Kingery and Smith, 1985, Kingery and Vandiver, 1986). (b) Isothermal section at 1100ºC of the phase diagram shown on the left. The composition of 17 French soft paste porcelains are shown in the compositional triangle [β-wollastonite, CS] + [SiO_2 phase (cristobalite or tridymite)] + [liquid] of composition **3**. The backscattered electron image shows large subidiomorphic tridymite laths and tiny wollastonite grains as crystallization products from the 1100ºC melt (now glassy matrix), contrasting with a relict α-quartz particle (upper right corner), surrounded by the characteristic crack due to the crystallographic β/α-inversions during cooling (Heimann and Maggetti, 2014).

expected to consist of [β-wollastonite] + [tridymite/cristobalite] + [liquid of composition 3]. However, when the kiln cools, the composition of the liquid follows the curve to the peritectic point 1, at which point simultaneously [β-wollastonite] and [tridymite/cristobalite] crystallize. The peritectic reaction [L] + [β-CS] → [NC_3S_6] + [SiO_2] starts at 1035ºC and consumes all remaining liquid, leading to the final equilibrium phase association [β-wollastonite] + [devitrite] + [tridymite/cristobalite].

The microstructure of typical Sèvres soft-paste porcelain (Fig. 27, centre) shows quartz grains, partially or completely transformed to tridymite/cristobalite, wollastonite and glass. Although the equilibrium phases tridymite and wollastonite are present as expected from the phase diagram, devitrite is conspicuously absent. Devitrite is sometimes found as an unwanted devitrification product of modern soda-lime-silica sheet glass, but is readily resorbed in the glass matrix after prolonged heating to high temperatures (Aboud *et al.*, 2005), in accord with the findings above. The surviving large amount of a non-equilibrium glassy phase is due to the presence of alumina that inhibits devitrification.

5. Conclusion

Mineralogical investigations of ancient and historical ceramics provide a sensitive probe to gauge the technical competence of potters as well as the overall state of technological development of a particular society. The study of the microstructure of ancient and historical ceramics provides many ways to determine how effectively craftspeople responded to the challenge of turning natural raw material 'clay' into the finished product 'pottery'. Plots of chemical composition of the original material as well as the mineralogical phase composition of the resulting product in ceramic phase diagrams show clearly how well the potter succeeded in the intuitive quest towards a stable phase equilibrium that would result in dense wares. As it turns out, for all Neolithic and most Bronze Age ceramics this quest was clearly not high on the agenda of the ancient potters, as their major goal was to produce porous vessel bodies for cooking pots, water containers to keep the water fresh and cool, or fermentation containers. Surface densification by burnishing vessels in the leather-hard state and, later, glazing would provide significant incentive for technological development toward surficially denser pottery without necessarily relying on higher firing temperatures. Indeed, at the rather low firing temperatures applied, most mineral-grain boundary reactions would have occurred far away from thermodynamic equilibrium, and hence were kinetically controlled. Kinetics exerts constraints on thermodynamics by retarding reaction rates because of low temperatures, large temperature gradients present in primitive pottery kilns, short reaction times, inhomogeneously distributed reaction partners, and varying redox conditions. Observation of mineral phases formed during ceramic firing such as diopside, gehlenite, anorthite, sanidine or mullite can tell the ceramics analyst how well the starting clay was processed and how efficiently high heat could be generated in ever more sophisticated pottery kilns; eventually leading to very high fired, dense and translucent porcelain.

The microstructural analyses of ancient pottery, assisted by ceramic phase diagrams, show impressively how the intellectual environment, *i.e.* the technological knowledge of a particular ancient society filled the requirements of the cultural environment (Kolb, 1982), *i.e.* individual needs by optimum exploitation and manipulation of raw materials extracted from the natural environment (Stimmell *et al*., 1982; Heimann, 1989).

References

Aboud, T.K., Stoch, L. and Sroda, M. (2005) Quartz crystallization in soda-lime-silica glass. *Optica Applicata*, **35**, 829–836.

Andersen, D.J., Lindsley, D.H. and Davidson, P.M. (1993) QUILF: a Pascal program to assess equilibria among Fe-Mg-Mn-Ti oxides, pyroxenes, olivine, and quartz. *Computers and Geosciences*, **19**, 1333–1350.

Belfiore, C.M., Day, P.M., Hein, A., Kilikoglou, V., La Rosa, V., Mazzoleni, P. and Pezzino, A. (2007) Petrographic and chemical characterisation of pottery production of the Later Minoan I kiln at Haghia Triada, Crete. *Archaeometry*, **49**, 621–653.

Bemmann, H. (1993) Terra Sigillata – Tafelgeschirr der Römer und "Leitfossil" der Archäologie. In: *Die Römer in der Pellenz*, **2** (K. Schäfer, editor).

Boaretto, E., Wu, X., Yuan, J., Bar-Yosef, O., Chu, V., Pan, Y., Liu, K., Cohen, D., Jiao, T., Li, S., Gu, H.,

Goldberg, P. and Weiner, S. (2009) Radiocarbon dating of charcoal and bone collagen associated with early pottery at Yuchayan Cave, Hunan Province, China. *Proceedings of the National Academy of Sciences of the USA*, **106**, 9595–9600.

Bowen, N.L. (1915) The crystallization of haplobasaltic, haplodioritic and related magmas. *American Journal of Science*, **40**, 161–185.

Brongniart, A. (1844) *Traité des Arts Céramiques ou des Poteries considérées dans leur Histoire, leur Pratique et leur Théorie*. 3 vols and 1 atlas, Paris: Béchet Jeune; 2nd edn reviewed, corrected and augmented with notes and additions by A. Salvetat, Paris: Béchet Jeune, 1854; 3rd edn with notes and additions by A. Salvetat, 1877; facsimile of the 3rd edn. Paris: Dessain and Tolra, 1977.

Chard, C.S. (1974) *Northeast Asia in Prehistory*. University of Wisconsin Press, Madison, Wisconsin, USA.

Chatterjee, N.D., Krüger, R., Haller, G. and Olbricht, W. (1998) The Bayesian approach to an internally consistent thermodynamic database: theory, database, and generation of phase diagrams. *Contributions to Mineralogy and Petrology*, **133**, 149–168.

Clark, S.P., Schairer, J.F. and de Neufville, J. (1962) Phase relations in the system $CaMgSi_2O_6$–$CaAl_2Si_2O_8$–SiO_2 at low and high pressure. *Carnegie Institute of Washington, Year Book*, **61**, 59–68.

Cultrone, G., Rodriguez-Navarro, C., Sebastian, E., Cazalla, O. and De la Torre, M.J. (2001) Carbonate and silicate phase reactions during ceramic firing. *European Journal of Mineralogy*, **13**, 621–634.

Déchelette, J. (1904) *Les Vases céramiques ornés de la Gaul romains (Narbonnaise, Aquitaine et Lyonnaise)*. A. Picard and fils, Paris.

Dondi, M., Ercolani, G., Fabbri, B., and Marsigli, M. (1998) An approach to the chemistry of pyroxenes formed during the firing of Ca-rich silicate ceramics. *Clay Minerals*, **33**, 443–452.

Dragendorff, H. (1895/96) Terra Sigillata. Ein Beitrag zur Geschichte der griechischen und römischen Keramik. *Bonner Jahrbücher*, **96/97**, 18–155.

Escardino, A., García-Ten, J. and Soriano, M. (2006) Study of calcite decomposition during wall tile firing. *Qualicer* 2006, 265–278.

Franklin, U.M. (1980) *The potential of technical studies*. Paper presented at the Symposium on the Bronze Age of China. New York, June 2-3, 1980.

Gibbs, J.W. (1878) On the equilibrium of heterogeneous substances. *Transactions of the Connecticut Academy of Arts and Science*, **3**, 108–248, 343–524.

Goldschmidt, V.M. (1911) Anwendung der Phasenregel auf Silikatgesteine. *Zeitschrift für Elektrochemie*, **17**, 686–689.

Goldsmith, J.R. (1953) A "simplexity principle" and its relation to "ease" of crystallization. *Bulletin of the Geological Society of America*, **64**, 439–451.

Görres, M., Evangelakakis, C., Kroll, H. and Kohl, V. (2000) The application of mineralogical techniques to the characterization of archaeological ceramic finds. Pp. 985–988 in: *Applied Mineralogy; In Research, Economy, Technology, Ecology and Culture* (D. Rammlmair, editor). Balkema, Rotterdam, The Netherlands.

Grapes, R. (2006): *Pyrometamorphism*. Springer, Berlin.

Hamdan, M.A., Martinez, S.M., Garcia Vallès, M.T., Nogués, J.M., Hassan, F.A., Flower, R.J., Aly, M.H., Senussi, A. and Ebrahim, E.S. (2014) Ancient Egyptian pottery from the subsurface floodplain of the Saqqara-Memphis area: its mineralogical and geochemical implications. *Archaeometry*, **56**, 987–1008.

Hängst, K. (1979) *Mineralogische Untersuchungen an altägyptischer Keramik der 18. und 19. Dynastie*. Unpublished Masters thesis, Universität Köln, Germany.

Heimann, R.B. (1978/79) Mineralogische Vorgänge beim Brennen von Keramik und Archäothermometrie. *Acta Praehistorica and Archaeologica*, **9/10**, 79–102.

Heimann, R.B. (1982) Firing technologies and their possible assessment by modern analytical methods. Pp. 89–96 in: *Archaeological Ceramics* (J.S. Olin and A.D. Franklin, editors). Smithsonian Institution Press, Washington, D.C.

Heimann, R.B. (1989) Assessing the technology of ancient pottery: The use of ceramic phase diagrams. *Archeomaterials*, **3**, 123–148.

Heimann, R.B. (1991) Technological progress and market penetration of advanced ceramics in Canada. *Bulletin of the American Ceramic Society*, **70(7)**, 1120–1124.

Heimann, R.B. (2010) *Classic and Advanced Ceramics. From Fundamentals to Applications*, Wiley-VCH Verlag GmbH, Weinheim, Germany.

Heimann, R.B. (2016) X-ray powder diffraction. Chapter 19 in: *Oxford Handbook of Archaeological Ceramic Analysis (*A.M.W. Hunt, editor). Oxford University Press, Oxford, UK, 768 pp.

Heimann, R.B. and Franklin, U.M. (1979) Archaeo-thermometry: The assessment of firing temperatures of ancient ceramics. *Journal of the International Institute of Conservation, Canadian Group (IICCG)*, **4(2)**, 23−45.

Heimann, R.B. and Maggetti, M. (1981) Experiments on simulated burial of calcareous terra sigillata (mineralogical change). Preliminary results. Pp. 163−177 in: *Scientific Studies in Ancient Ceramics*, occasional paper no. 19. British Museum Research Laboratory, London.

Heimann, R.B. and Maggetti, M. (2014) *Ancient and Historical Ceramics. Materials, Technology, Art, and Culinary Traditions*. Schweizerbart Science Publishers, Stuttgart, Germany.

Heimann, R.B., Maggetti, M. and Einfalt, H.C. (1980) Zum Verhalten des Eisens beim Brennen eines kalkhaltigen illitischen Tons unter reduzierenden Bedingungen. *Berichte der Deutschen Keramischen Gesellschaft*, **57**, 145−152.

Huebner, J.S. (1971) Buffering techniques for hydrostatic systems at elevated temperatures. Pp. 123−127 in: *Research Techniques for High Pressure and High Temperatures* (G.C. Ulmer, editor). Springer, Berlin, Heidelberg, New York.

Huysecom, E., Rasse, M., Lespez, L., Neumann, K., Fahmy, A., Ballouche, A., Ozainne, S., Maggetti, M., Tribolo, Ch. and Soriano, S. (2009) The emergence of pottery in Africa during the tenth millennium cal BC: new evidence from Ounjougou (Mali). *Antiquity*, **83**, 905−912.

Iqbal, Y. and Lee, W.E. (1999) Fired porcelain microstructures revisited. *Journal of the American Ceramic Society*, **81**, 3584−3590.

Iqbal, Y., and Lee, W.E. (2000) Microstructural evolution in triaxial porcelain. *Journal of the American Ceramic Society*, **83**, 3121−3127.

Jabbori, S. (1980) Report on geological investigation of clay deposits for brick industry in Nahrawan area with reserve estimation. *GEOSURV, Internal Rept*. No. 1039.

Jordan, P. and Zvelebil, M. (editors) (2009) *Ceramics before Farming: The Dispersal of Pottery Among Prehistoric Eurasian Hunter-gatherers*. University College London Institute of Archaeology, Publication **53** and Left Coast Press, Walnut Creek, California, USA.

Kadum, L.S. and Hussain, A.I. (2011) Origin and mineralogy of construction materials of gravel and sand in Tikrit area. *Tikrit University Journal for Humanities*, **18(8)**, 33−46.

Kattner, U.R. (1997) The thermodynamic modeling of multicomponent phase equilibria. *JOM*, **49(12)**, 14−19.

Kilb, L. (1979) *Gefügeanalytische Untersuchungen historischer steinzeugartiger Werkstoffe zur Behandlung archäometrischer Fragestellungen*. Unpublished Ph.D. dissertation. Technical University Clausthal-Zellerfeld, Germany.

Kilikoglou, V., Vekinis, G. and Maniatis, Y. (1995) Toughening of ceramic earthenware by quartz inclusions: an ancient art revisited. *Acta Metallurgica et Materialia*, **43**, 2959−2965.

Kilikoglou, V., Vekinis, G., Maniatis, Y. and Day, P.M. (1998) Mechanical performance of quartz-tempered ceramics. Part I: Strength and toughness. *Archaeometry*, **40**, 261−279.

Kingery, W.D. and Smith, D. (1985) The development of European soft-paste (frit) porcelain. Pp. 273−292 in: *Ancient Technology to Modern Science*. Ceramics and Civilization, vol. I, The American Ceramic Society, Columbus, Ohio, USA.

Kingery, W.D. and Vandiver, P.B. (1986) *Ceramic Masterpieces. Art, Structure, and Technology*. The Free Press, New York.

Kingery, W.D., Bowen, H.K. and Uhlmann, D.R. (1976) *Introduction to Ceramics*. 2nd edition John Wiley & Sons, New York, Chichester, Brisbane, Toronto, Singapore.

Klein, R. (1980) Later Pleistocene hunters. Pp. 90−91 in: *The Cambridge Encyclopedia of Archaeology* (A. Sherratt, editor). Prentice Hall of Canada Ltd., Scarborough, Ontario, Canada.

Klima, B. (1962) The first ground plan of an Upper Palaeolithic loess settlement in Middle Europe and its meaning. Pp. 193−210 in: *Courses Towards Urban Life* (R.J. Braidswood and G.R. Willey, editors). Chicago University Press, Chicago.

Knorr, R. (1919) *Töpfer und Fabriken verzierter Terra-Sigillata des 1. Jahrhunderts*. W. Kohlhammer, Stuttgart.

Kockelmann, W., Kirfel, A. and Hähnel, E. (2001) Non-destructive phase analysis of archaeological ceramics using TOF neutron diffraction. *Journal of Archaeological Science*, **28**, 213–222.

Kolb, C.C. (1982) Ceramic technology and problems and prospects of provenience in specific ceramics from Mexico and Afghanistan. Pp. 193–208 in: *Archaeological Ceramics* (J.S. Olin and A.D. Franklin, editors). Smithsonian Institution Press, Washington, D.C.

Lee, W.E. and Iqbal, Y. (2001) Influence of mixing on mullite formation in porcelain. *Journal of the European Ceramic Society*, **21**, 2583–2586.

Letsch, J. and Noll, W. (1983) Phase formation in several ceramic subsystems at 600ºC–1000ºC as a function of oxygen fugacity. *Ceramic Forum International/Berichte der Deutschen Keramischen Gesellschaft*, **60**, 259–267.

Levin, E.M., Robbins, C.R. and McMurdie, H.F. (1964–1990) *Phase Diagrams for Ceramists*. Vol. I – VIII. The American Ceramic Society, Westerville, Ohio, USA.

Louisnathan, S.J. (1971) Refinement of the crystal structure of a natural gehlenite, $Ca_2Al(Al,Si)_2O_7$. *The Canadian Mineralogist*, **10**, 822–837.

Maggetti, M. (1982) Phase analysis and its significance for technology and origin. Pp. 121–133 in: *Archaeological Ceramics* (J.S. Olin and A.D. Franklin, editors). Smithsonian Institution, Washington, D.C.

Maggetti, M. (1986) Majolika aus Mexiko-ein archäometrisches Fallbeispiel. *Fortschritte der Mineralogie*, **64**, 87–103.

Maggetti, M. (2001) Chemical analyses of ancient ceramics: What for? *CHIMIA International Journal of Chemistry*, **55**, 923–930.

Maggetti, M. and Galetti, G. (1986) Chemischer Herkunftsnachweis der "Schwarzen Sigillata" vom Magdalensberg. *Magdalensberg-Grabungsbericht*, **15**, 391–431.

Maggetti, M. and Heimann, R.B. (1979) Bildung und Stabilität von Gehlenit in römischer Feinkeramik. *Schweizer Mineralogische und Petrographische Mitteilungen*, **59**, 413–417.

Maggetti, M. and Küpfer, T. (1978) Composition of the Terra Sigillata from La Péniche (Vidy, Lausanne, Switzerland). *Archaeometry*, **20**, 183–188.

Maggetti, M., Neururer, Ch. and Ramseyer, D. (2011) Temperature evolution inside a pot during experimental surface (bonfire) firing. *Applied Clay Science*, **53**, 500–508.

Maniatis, Y. and Tite, M.S. (1975) A scanning electron microscopic examination of the bloating of fired clay. *Transactions of the British Ceramic Society*, **74**, 229–232.

Morey, G.W. and Bowen, N.L. (1925) The system sodium metasilicate–calcium metasilicate–silica. *Journal of the Society of Glass Technology*, **9**, 232–233.

Mustafa, M.M. (2011) Mineral resources and industrial deposits in the Mesopotamian plain. *Iraqi Bulletin of Geology and Min*eralogy, Special issue **4**, 105–118.

Nakamura, T., Taniguchi, Y., Tsuji, S. and Oda, H. (2001) Radiocarbon dating of charred residues on earliest pottery in Japan. *Radiocarbon*, **43**, 1129–1138.

Niggli, P. (1954) *Rocks and Mineral Deposits*. Pp. 347–427. Freeman & Company, San Francisco, California, USA.

Noll, W. (1982) Mineralogie und Technik der Keramiken Altkretas. *Neues Jahrbuch der Mineralogie, Abhandlungen,*. **143(2)**, 150–199.

Noll, W. (1984) Antike Keramik und ihre Dekoration in naturwissenschaftlicher Sicht. Pp. 42–53 in: *International Vase Symposium, Amsterdam*. Allard Pierson Series, Vol 5.

Noll, W. (1991) *Alte Keramiken und ihre Pigmente*. E. Schweizerbart, Stuttgart. 334 pp.

Noll, W. and Heimann, R.B. (2016) *Ancient Old World Pottery. Materials, Technology, and Decoration*. Schweizerbart Science Publishers, Stuttgart, Germany. 311 pp.

Osborn, E.F. and Tait, D.B. (1952) The system diopside–forsterite–anorthite. *American Journal of Science*, Bowen volume, 413–433.

Peters, T. and Iberg, R. (1978) Mineralogical changes during firing of calcium-rich brick clays. *Bulletin of the American Ceramic Society*, **57**, 503–509.

Picon, M., Vichy, M. and Meille, E. (1971) Composition of Lezoux, Lyon and Arezzo Samian ware. *Archaeometry*, **13**, 191–208.

Powell, A.J., McDonnell, J.G., Batt, C.M. and Vernon, R.W. (2002) An assessment of the magnetic response of an iron-smelting site. *Archaeometry*, **44**, 651–665.

Rankin, G.A. and Wright, F.E. (1915) The ternary system $CaO–Al_2O_3–SiO_2$. *American Journal of Science*, **39**, 1–79.

Rehak, P., Kunath-Fandrel, G., Losso, P., Hildmann, B., Schneider, H. and Jäger, C. (1998) Study of the Al coordination in mullite with varying Al:Si ratio by ^{27}Al NMR spectroscopy and X-ray diffraction. *American Mineralogist*, **83**, 1266–1276.

Roberts, P. (1997) Mass-production of Roman finewares. Pp. 188–193 in: *Pottery in the Making. World Ceramic Traditions* (I. Freestone and D. Gaimster, editors), British Museum Press. London.

Rodriguez-Navarro, C., Ruiz-Agudo, E., Luque, A., Rodriguez-Navarro, A. and Ortega-Huerto, M. (2009) Thermal decomposition of calcite: Mechanisms of formation and textural evolution of CaO nanocrystals. *American Mineralogist*, **94**, 578–593.

Rosenberger, F. (1979) *Fundamentals of Crystal Growth I*. Springer, Berlin.

Salmang, H., Scholze, H. and Telle, R. (2007) *Keramik*. 7th edition. Springer, Berlin, Heidelberg. 1148 pp.

Schairer, J.F. and Bowen, N.L. (1947) Melting relations in the systems $Na_2O-Al_2O_3-SiO_2$ and $K_2O-Al_2O_3-SiO_2$. *American Journal of Science*, **245**, 193–204.

Schneider, G. and Daszkiewicz, M. (2006) Chemical analysis of Italian Sigillata from Italy and from the northern provinces Pp. 537–543 in: *Old Pottery in a New Century – Innovating Perspectives on Roman Pottery Studies* (D. Malfitano, J. Poblome and J. Lund, editors). *Atti del Convegno Internazionale di Studi*, Catania, 22-24 Aprile.

Schneider, G. and Hoffmann, B. (1990) Chemische Zusammensetzung italischer Sigillata. Pp. 27–38 in: *Conspectus formarum terrae sigillatae italico modo confactae*. Materialien zur römisch-germanischen Keramik (E. Ettlinger *et al*., editors), Bd. 10. Bonn, Germany.

Schneider, G., Knoll, H., Gallis, K. and Demoule, J.P. (1990) Production and circulation of Neolithic Thessalian pottery: Chemical and mineralogical analyses. In: *La Thessalie, Quinze années de recherchés archeologiques*, *1975-1990*. Actes du Colloque International, Lyon, France.

Schneider, G., Knoll, H., Gallis, K. and Demoule, J.P. (1991) Transition entre les cultures néolithiques des Sesklo et de Dimini: Recherches minéralogiques, chimiques et technologiques sur les ceramiques et les argiles. *Bulletin de Correspondence Héllenique* (BCH), **115**, 1–64.

Schroeder, P.A. and Erickson, G. (2014) Kaolin: From ancient porcelain to nanocomposites. *Elements*, **10**, 177–182.

Schüller, K.H. (1964) Reactions between mullite and glassy phase in porcelains. *Transactions of the British Ceramic Society*, **63**, 103–117.

Schüller, K.H. (1982) The development of microstructures in silicate ceramics. 1. Whitewares. *Journal of Educational Modules in Materials Science and Engineering*, **4**, 529–565.

Schultz, A. and Chang, Y.A. (1985) Computer graphics for ternary phase diagrams. *Journal of Metals*, November, 10–13.

Shaw, J.C. (2008) *Northern Thai Ceramics*. 2nd edition. Duangphorn Kemasingki, Chiang Mai, Thailand.

Shaw, J.C. (2009) *Thai Ceramics*. Citylife Publications, Chiang Mai, Thailand.

Smith, J.V. (1959) The crystal structure of proto-enstatite, $MgSiO_3$. *Acta Crystallographica*, **12**, 515–519.

Stimmell, C., Heimann, R.B. and Hancock, R.G.V. (1982) Indian pottery from the Mississippi Valley: Coping with bad raw materials. Pp. 219–228 in: *Archaeological Ceramics* (J.S. Olin and A.D. Franklin, editors). Smithsonian Institution Press, Washington, D.C.

The American Ceramic Society (1992–1996) *Phase Equilibria Diagrams*. Vol. IX-XII. The American Ceramic Society, Westerville, Ohio, USA.

Tilley, C.E. (1938) Aluminous pyroxenes in metamorphosed limestones. *Geological Magazine*, **75**, 81–86.

Tite, M.S., Freestone, I.C., Meeks, N.D. and Bimson, M. (1982) The use of scanning electron microscopy in the technological examination of ancient ceramics. Pp. 109–120 in: *Archaeological Ceramics* (J.S. Olin and A.D. Franklin, editors). Smithsonian Institution Press, Washington.

Tite, M.S., Freestone, I.C. and Wood, N. (2012) An investigation into the relationship between the raw materials used in the production of Chinese porcelain and stoneware bodies and the resulting microstructures. *Archaeometry*, **54**, 37–55.

Ullrich, B. and Ballmair, H. (2002) Fuldaer und Meissener Porzellan des späten 18. Jahrhunderts: ein technikhistorischer Vergleich, *Beiträge zur Naturkunde in Osthessen*, **38**, 5–13.

Ullrich, B., Lange, P. and Kerbe, F. (2010) Thüringer und Meissener Porzellan des späten 18. und frühen 19. Jahrhunderts – ein werkstoffhistorischer Vergleich. Pp. 281–289 in: *Porzellanland Thüringen, 250 Jahre Porzellan aus Thüringen*, Museumsverband Thüringen e.V.

Wachtman, J.B. (1969) *Mechanical and Thermal Properties of Ceramics*. National Bureau of Standards special publication, vol. 303. US Department of Commerce, NBS. 268 pp.

Walcha, O. (1981) *Meissen Porcelain*. G.P. Putnam's Sons, New York. 516 pp.

West, D.R.F. (1982) *Ternary Phase Diagrams*. 2nd edition. Chapman & Hall, London, New York.

Wijnen, M.H.J.M.N. (1981) The Early Neolithic I settlement at Sesklo: an early farming community in Thessaly, Greece. *Analecta Praehistorica Leidensia*, **XIV**, 1–146.

Williams, D. (1997) Ancient Greek pottery. Pp. 86–91 in: *Pottery in the Making. World Ceramic Traditions* (I. Freestone and D. Gaimster, editors), British Museum Press, London.

Wood, N. and Rastelli, S. (2014) Parallel developments in Chinese porcelain technology in the 13th–14th centuries AD. Pp. 225–234 in: *Craft and Science: International Perspectives on Archaeological Ceramics* (M. Martinón-Torres, editor), Bloomsbury Qatar Foundation, Doha, Qatar. http://dx.doi.org/10.5339/uclq.2014.cas.ch24.

Yin, M., Rehren, Th. and Zheng, J. (2011) The earliest high-fired glazed ceramics in China: The composition of the proto-porcelain from Zhejiang during the Shang and Zhou periods (c.1700–221 BC). *Journal of Archaeological Science*, **38**, 2352–2365.

Zanelli, C., Raimondo, M., Guarini, G. and Dondi, M. (2011)The vitreous phase of porcelain stoneware: composition, evolution during sintering and physical properties. *Journal of Non-Crystalline Solids*, **357**, 3251–3260.